

# Chem Soc Rev

This article was published as part of the  
2009 Themed issue dedicated to  
Professor Jean-Pierre Sauvage

Guest editor Professor Philip Gale

Please take a look at the issue 6 [table of contents](#) to access  
the other reviews.



# Gold nanoparticles in nanomedicine: preparations, imaging, diagnostics, therapies and toxicity†

Elodie Boisselier and Didier Astruc\*

Received 12th January 2009

First published as an Advance Article on the web 21st April 2009

DOI: 10.1039/b806051g

This critical review provides an overall survey of the basic concepts and up-to-date literature results concerning the very promising use of gold nanoparticles (AuNPs) for medicinal applications. It includes AuNP synthesis, assembly and conjugation with biological and biocompatible ligands, plasmon-based labeling and imaging, optical and electrochemical sensing, diagnostics, therapy (drug vectorization and DNA/gene delivery) for various diseases, in particular cancer (also Alzheimer, HIV, hepatitis, tuberculosis, arthritis, diabetes) and the essential *in vitro* and *in vivo* toxicity. It will interest the medicine, chemistry, spectroscopy, biochemistry, biophysics and nanoscience communities (211 references).

## 1. Introduction

Medicinal problems are a quest of all civilizations. Since nanoscience is one of the major areas of present scientific progress, it should shortly result in essential advancement for the benefit of human health. The biomedical applications of metal nanoparticles started in the 1970s with the use of nanobioconjugates after the discovery of immunogold labeling by Faulk and Taylor.<sup>1</sup> Traditional imaging techniques remain crucial in diagnostic, and AuNPs proves to be superior to classic chemicals. Subsequently, nanostructures have been introduced in a broad range of biological applications.<sup>2–5</sup> Supramolecular chemistry principles have also catalyzed major advances in this area including both imaging and sensors using biological host–guest recognition of biomolecules.<sup>6</sup> Presently, research is now also emphasizing drug vectorization<sup>7–9</sup> along with physical methods such as electron microscopy and spectroscopy.<sup>10</sup> Nanotechnology is

bringing a key contribution, a crucial property being the plasmon absorption and scattering of AuNPs. It is involved particularly in both the photodiagnostics and photothermal therapy of cancers and other main diseases.<sup>8</sup> The goal of drug vectorization, promised to a bright future, is to diminish or suppress side effects due to toxicity, improve therapeutic efficiency and biodistribution, and overcome the problems of solubility, stability and pharmacokinetics of drugs.<sup>9,10</sup>

In this critical review, we will concentrate our attention on AuNPs, also including non-spherical AuNPs, in biochemistry and nanomedicine with emphasis on the above areas. This broad field presently involves a considerably increasing number of publications, thus we will focus on major ideas and most recent studies.

## 2. Gold nanoparticles (AuNPs) and bioconjugate chemistry

Gold was discovered in Bulgaria five thousand years ago, and the ancient colloidal gold must have first appeared in antiquity in China and Egypt for therapeutic and decorative purposes. A famous example is the Lycurgus cup, from the 4th century, visible at the British Museum in London. Gold colloids have

Institut des Sciences Moléculaires, UMR CNRS No. 5255,  
Université Bordeaux I, 33405, Talence Cedex, France.  
E-mail: d.astruc@ism.u-bordeaux1.fr

† Dedicated to our distinguished colleague Dr Jean-Pierre Sauvage at the occasion of his 65th birthday.



Elodie Boisselier

Elodie Boisselier obtained her bachelor of science degree in biochemistry from the Université Bordeaux II. She is presently studying for a PhD under the guidance of Professor Didier Astruc at the Université Bordeaux I in the area of Au nanoparticles. Her interests are in the synthesis and biomedical applications of Au nanoparticles.



Didier Astruc

Didier Astruc is Professor of Chemistry at the Université Bordeaux I and Member of the Institut Universitaire de France. He did his PhD in Rennes with R. Dabard and his postdoctoral work at MIT with R. R. Schrock. His present interests are in dendrimers and nanoparticles and their applications in catalysis, molecular materials science, and nanomedicine.

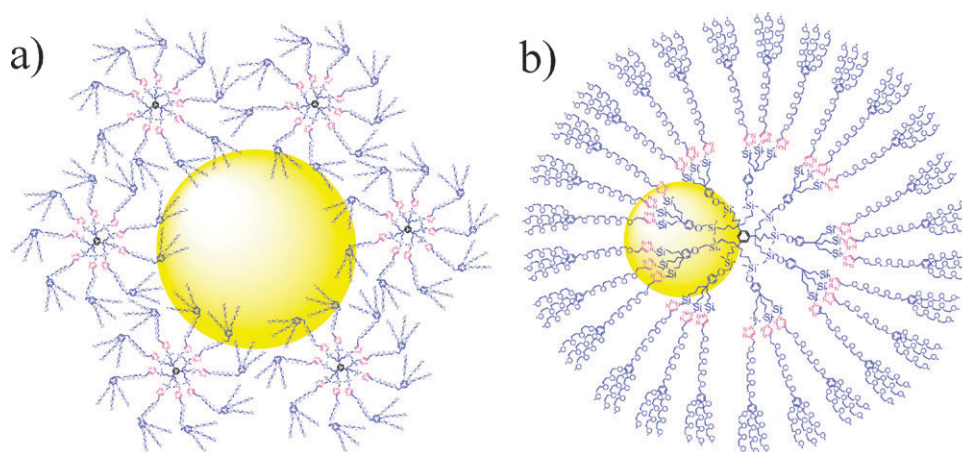


**Fig. 1** (a) AuNPs stabilized by several  $G_0$  dendrimers; (b)  $G_1$ -dendrimer-encapsulated AuNPs. Reprinted with permission of the Royal Society of Chemistry (ref. 24, Astruc's group).

been recommended for curing various diseases over the centuries and till recently, although the mechanisms of action are still poorly understood. In 1857, Faraday reported the first scientific article on AuNPs, attributing the red color to the colloidal nature of AuNPs,<sup>11</sup> and in 1908 Mie rationalized their visible absorption using Maxwell's electromagnetic equations.<sup>12</sup> AuNPs are available in the range from 1 to more than 120 nm, and their plasmon band visible absorption can be observed above 3 nm (*vide infra*). They disclose considerable applications in optics, catalysis, materials science and nanotechnology also including biology and nanomedicine.<sup>13</sup>

There are a large number of ways to synthesize AuNPs most of the time starting from commercial  $\text{HAu}^{\text{III}}\text{Cl}_4$ .<sup>14</sup> Citrate reduction of  $\text{Au}^{\text{III}}$  to  $\text{Au}^0$  in water was introduced by Turkevitch *et al.* in 1951,<sup>15</sup> a method that is still used nowadays to subsequently replace the citrate ligand of these AuNPs by appropriate ligands of biological interest.<sup>13</sup> Recent modifications of the Turkevitch method have allowed better size distribution and size control within the 9–120 nm range.<sup>16</sup>

Although AuNPs can be stabilized by a large variety of stabilizers (ligands, surfactants, polymers, dendrimers, biomolecules, *etc.*),<sup>13</sup> the most robust AuNPs were disclosed by Giersig and Mulvaney to be stabilized by thiolates using the strong Au–S bond between the soft acid Au and the soft thiolate base.<sup>17</sup> Along this line, by far the most popular synthetic method using such sulfur coordination for AuNP stabilization is the Shiffrin–Brust biphasic synthesis using  $\text{HAuCl}_4$ , a thiol, tetraoctylammonium bromide and  $\text{NaBH}_4$  in water–toluene yielding thiolate-AuNPs.<sup>18</sup> Functional thiolates can also be introduced using this method or upon subsequent bimolecular substitution of a thiolate ligand by such a functional thiol:<sup>19</sup>



Oligonucleotides, peptides and PEGs are easily attached to AuNPs in this way. Since the solubility of these AuNPs is controlled by the solubilizing properties of the terminal group of the thiolate ligands, AuNPs can be transferred from an aqueous phase to an organic phase or *vice versa* by appropriate ligand exchange. Water-soluble AuNPs typically

contain terminal carboxylate groups at their periphery. The carboxy group is used to attach the amino groups of biomolecules using 1-ethyl-3-(3-dimethylaminopropyl)-carbodiimide-HCl abbreviated EDC (bioconjugate chemistry).<sup>20</sup>

Another useful protocol consists in using the famous “click” reaction linking a terminal alkyne and an azide.<sup>21</sup> The excellent efficiency of this method has recently been demonstrated.<sup>22</sup> A way to form AuNPs made of a precise number of metal atoms consists in using dendrimers containing a pre-organized number of internal ligands, which leads to dendrimer-encapsulated AuNPs (Fig. 1).<sup>23,24</sup> Super robust AuNPs, stable in the pH 1–14 range and under NaCl concentrations up to 5 M, were synthesized using PEG sorbitan fatty acid esters functionalized with lipoic acid. These scaffolds show both strong coordination through the chelating thiols and van der Waals interactions.<sup>25</sup>

Very interestingly, not only spherical AuNPs are synthesized, but also the shapes of the nanoparticles can be varied using appropriate techniques. In particular, Au nanorods (AuNRs) with controlled aspect ratio (*i.e.* the ratio of the length along the long axis to the short axis) in the range of 2–6 have been synthesized using the micelle-templated seed and feed technique developed by the groups of Murphy<sup>26</sup> (Fig. 2) and El Sayed,<sup>27</sup> and the Halas' group has developed the synthesis of Au nanoshells (AuNSs) composed of a silica core (100–200 nm in diameter) surrounded by a thin Au layer (5–20 nm).<sup>28</sup> Citrate-capped AuNPs and AuNSs as well as cetyl trimethylammonium bromide (CTAB)-capped AuNRs are not stable in the presence of a buffer solution, because salt ions have an aggregating effect, but these AuNPs are readily stabilized by thiol-functionalized PEG ligands.<sup>29</sup> The Murphy group has successfully engineered the surface chemistry of AuNRs. Thus, long AuNRs were obtained (500 nm long, 20 nm wide). The cationic surfactant used in the synthesis remains on the sides of the AuNR in the form of a bilayer resulting in a cationic charge to the AuNR, leaving the AuNR ends available for subsequent reaction. Bifunctional thiols such as biotin-disulfide can be bound to the Au(111) crystal face on the AuNR ends, whereas the CTAB bilayer is maintained on the AuNR sides. Addition of streptavidin further leads to end-to-end linkage of the AuNRs. Similarly,

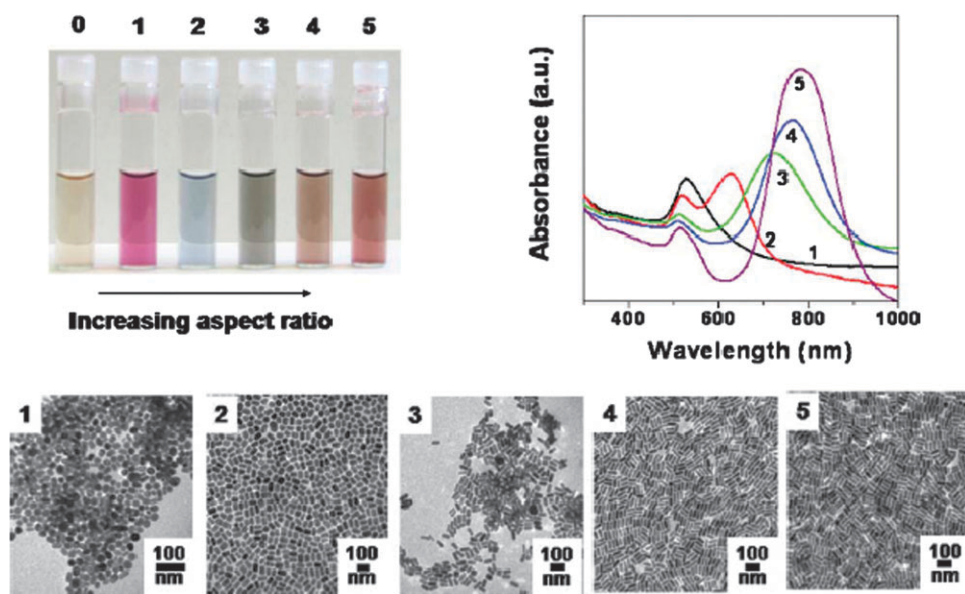


**Fig. 2** The optical properties of gold and silver nanoparticles change drastically with nanoparticle shape. The photograph shows aqueous solutions of 4 nm gold nanospheres (vial 0) and progressively higher aspect ratio gold nanorods (1–5). The optical spectra and transmission electron micrographs for the particles in vials 1–5 are also shown. Scale bars in micrographs are all 100 nm. Reprinted with permission of the Royal Society of Chemistry (ref. 26, Murphy's group).

mercaptopropionic acid preferentially binds the AuNR ends leading to end-to-end bonded AuNRs linked by hydrogen bonds. Upon using Ag(I),<sup>26</sup> Guyot-Sionnest also grew AuNRs, because Ag(I) selectively slows down the growth of these AuNRs at faces that are less energetically favorable with “under-potential” Ag(0) deposition.<sup>30</sup>

In summary, the affinity of the surface of AuNPs having various sizes and shapes for thiols, disulfides, dithiocarbamates and amines allows facile bioconjugation with a variety of biomolecules. In particular, AuNPs conjugation with thiolated PEG masks them from the intravascular immune system and multifunctionalization for drug delivery is possible.<sup>31</sup> Since surfactants including CTAB have been found to be cytotoxic, other types of stabilization have been searched. For instance non-toxic liquid crystals have been used especially if the NaBH<sub>4</sub> reduction that leaves boride contamination can be avoided. Thus, liquid-chlorin photosensitizers based on purpurin-18 from green algae *Spirulina maxima* and choline hydroxide were recently used to synthesize AuNPs in the absence of surfactant and other reducing agent.<sup>32</sup>

### 3. The surface plasmon resonance (SPR) of AuNPs

According to the Mie theory,<sup>12</sup> an electromagnetic frequency induces a resonant coherent oscillation of the free electrons, called the surface plasmon resonance (SPR), at the surface of a spherical NP if it is much smaller than the light wavelength. This absorption lies in the visible region for Au, Ag and Cu. For metal nanoparticles, the localized surface plasmon resonance results in an enhanced electromagnetic field at the metal nanoparticle surface. The plasmon resonance of AuNPs<sup>32</sup> is observed down to 3 nm diameter, below which the AuNP can no longer be considered as a piece of metal with

a conduction band but becomes a molecule depicted by molecular orbitals (then the term cluster should be used rather than nanoparticle). As a result, an enhanced electromagnetic field appears at the AuNP surface above this size allowing surface-enhanced optical properties revealed using spectroscopic techniques. Thus, the extinction coefficients of the SPR bands are extremely high, up to  $10^{11} \text{ M}^{-1} \text{ cm}^{-1}$ , which is several orders of magnitude larger than those of all the organic dyes. AuNPs give rise to both absorption and scattering whose proportions depend on the AuNP size. AuNPs with a diameter smaller than 20 nm essentially show absorption, but size increase to 80 nm also increases the ratio of scattering to absorption. A high scattering cross section is indeed required for biological imaging based on light scattering.

For spherical AuNPs of 5 nm diameter, the surface plasmon band is located at 520 nm in ethanol, but it is very sensitive to the composition, size, shape, inter-particle distance and environment (dielectric properties) of the AuNPs. It is the high sensitivity to these factors that makes the basis of their use for biological labeling, detection, diagnostic and sensing. For instance, 5-nm AuNPs are orange-red, but they turn blue-purple upon aggregation (network formation) to larger AuNPs. Likewise, a change of refractive index of the solvent shifts the plasmon band. From the Mie theory, it follows that the frequency of the plasmon band varies from spherical to non-spherical nanoparticles of various shapes (rods, prisms, triangles, tetrapods, dogbones, cubes, shells). For instance, with AuNRs, two plasmon bands are observed, one corresponding to oscillations along the length of the AuNR (longitudinal plasmon band) and the other along the width of the AuNR (transverse plasmon band). The positions of these two bands vary with the AuNR aspect ratio. Thus AuNRs exhibit plasmon bands with maxima around 500 and

1600 nm. Since the ratio influences the position of the plasmon band absorption, the syntheses of AuNRs can be adjusted with suitable ratio so that they correspond to commercial lasers (e.g. 360 nm, 785 nm and 1064 nm). Moreover, the shift of the plasmon band to the near-IR region for AuNRs allows obtaining a penetration into living tissues that is much deeper than that of visible light and exciting less background fluorescence. In addition the multi-component plasmon absorption provides richer information than the single visible band of spherical AuNPs. Similarly, the plasmon band of AuNSs is shifted to the near-IR region and can be tuned by adjusting the ratio of the thickness of the AuNS to the diameter of the silica pore. The Halas group has shown that the smaller this ratio, the more redshifted is the plasmon absorption of the AuNS.<sup>28</sup>

## 4. Labeling and imaging

### 4.1 General: the techniques

Beside the most routine technique, transmission electron microscopy (TEM) that uses the high atomic weight of Au, several imaging techniques involve the surface plasmon band. Large AuNPs (>20 nm) can be imaged using an optical microscope in phase contrast or differential interference contrast mode. Detection with an optical microscope only involves scattered light in dark-field microscopy. Small AuNPs only absorb light, provoking heating of the environment that can be detected by photothermal imaging that record local variations of the refractive index by DIC microscopy or by photoacoustic imaging using heat-induced liquid expansion.

Other techniques are (i) fluorescence microscopy that allows detection at the single particle level, as the above plasmon-based techniques, (ii) photothermal coherence tomography (OCT) that is an optical analogue to ultrasound with relatively good penetration depth (1–2 mm) and resolution (1–10  $\mu\text{m}$ ),<sup>33</sup> (iii) multiphoton SPR microscopy (when illuminated by laser light in resonance with their plasmon frequency, these AuNPs generate an enhanced multiphoton signal measured in a laser scanning microscope),<sup>34</sup> (iv) X-ray scattering, involving better contrast AuNP agents than organic molecules with high signal-to-noise ratio with X-ray computer tomography, and (v) gamma radiation using neutron activation.<sup>20</sup>

The traditional application called immunostaining involves antibody-conjugated AuNPs that bind antigens of fixed, permeabilized cells thereby providing visualization by contrast using TEM. On the other hand, diluted AuNPs labeled with antibodies can label the outer cell surface without fixation and permeabilization, so that the inter-particle distance is larger than the optical resolution limit, which leads to single-particle imaging of cell movement. Receptor molecules that are bound to the membrane are observed in this way by time-resolved imaging within the cell membrane using the above optical techniques.<sup>20</sup> Magnetic Resonance Imaging (MRI) can be enhanced with or without gadolinium, and the main techniques are now discussed below.

In summary, facile bioconjugation and the variety of traditional and modern techniques including in particular the spectroscopic ones related to the plasmon resonance make

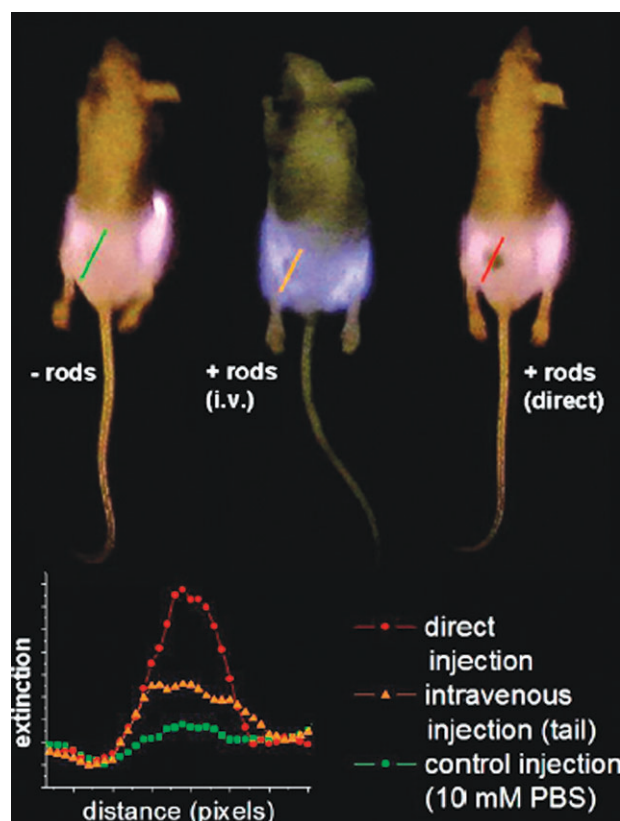


**Fig. 3** NIR transmission images of mice *prior* to PPTT treatments. Inset shows intensity line-scans of NIR extinction at tumor sites for control (■), intravenous (▲), and direct (●) administration of pegylated gold nanorods. Control mice were interstitially injected with 15  $\mu\text{L}$  10 mM PBS alone, while directly administered mice received interstitial injections of 15  $\mu\text{L}$  pegylated gold nanorods ( $\text{OD}_{\lambda=800} = 40$ , 2 min accumulation), and intravenously administered mice received 100  $\mu\text{L}$  pegylated gold nanorod ( $\text{OD}_{\lambda=800} = 120$ , 24 h accumulation) injections. Reprinted with permission of Elsevier (ref. 37, El Sayed's group).

AuNPs a remarkable up-to-date tool as imaging label and contrast agent (Fig. 3).

### 4.2 Enhancement of magnetic resonance imaging

The development of new contrast agents based on AuNPs for MRI is progressing fast. In addition to Gd chelates, several novel and highly efficient contrast agents were recently reported. The sensitivity of magnetic resonance imaging (MRI) can indeed be improved by using AuNPs as templating carriers of gadolinium chelates that are currently used for clinical diagnosis. Thus, the 2-nm-sized AuNPs carry about 150 ligands and exhibit a high relaxativity ( $r = 586 \text{ nM}^{-1} \text{ s}^{-1}$ ) as compared to  $3 \text{ nM}^{-1} \text{ s}^{-1}$  for the AuNP-free Gd chelate, which renders them very attractive as contrast agents for MRI (Fig. 4).<sup>35</sup>

The strong magnetism of magnetic NPs enhances MRI signals, and this property has recently been used. Iron oxide ( $\text{Fe}_3\text{O}_4$ ) embedded in AuNP shells appears to be useful for this purpose, because the iron oxide provides magnetism, whereas the Au shell allows to use the optical properties of AuNPs.<sup>36–38</sup> In another study, Co@Pt-AuNPs with enhanced magnetism

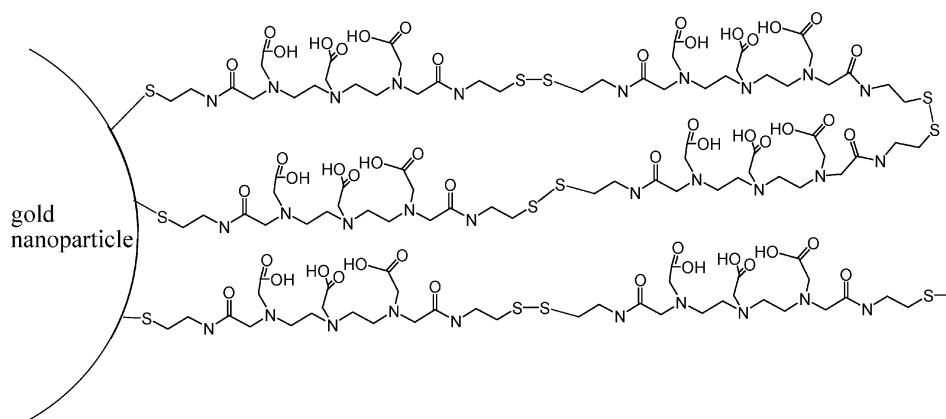


**Fig. 4** Schematic illustration of the DTDTPA shell grafted onto gold nanoparticles (Au@DTDTPA). Reprinted with permission of Wiley InterScience (ref. 35, Roux's group).

and high stability were used. Binding to this AuNP surface is ensured using lipoic acid connected to neutravidin that shows strong interaction with biotin. These Co@Pt-AuNPs serve as MRI agents to monitor the structural evolution of AB protofibrils, responsible for Alzheimer disease, in the early reversible stages. Magnetic NP-assisted MRI detection could also potentially be applied as sensitive probes of other proteins self-assemblies including prions,  $\alpha$ -synuclein and Huntingtin.<sup>39–41</sup>

### 4.3 Surface-enhanced Raman scattering (SERS)

Molecules located on the AuNP surface are submitted to the large field caused by the plasmon resonance of the AuNP up to a distance of approximately 10 nm at most from the AuNP surface. Among the different spectroscopic techniques that characterize the electromagnetic field resulting from the plasmon resonance of AuNPs (surface-enhanced fluorescence, surface-enhanced Rayleigh scattering, surface-enhanced absorption and surface-enhanced Raman scattering, SERS), SERS is most attractive, because of the huge enhancement of the SERS signal, by a factor of *ca.*  $10^{14}$ – $10^{15}$ , which improves the detection limit from ensembles of molecules to the single-molecule level. The Raman effect in molecules that are not located at a metal nanoparticle surface is normally weak, because visible light that is not absorbed by this molecule is only weakly inelastically scattered off the molecular vibrations. The selection rule for Raman spectroscopy is the polarizability change along the vibration, which usually provides only a weak Raman-active signal at usual concentration levels. Considerable enhancement occurs at the AuNP surface, however, because the intensity of the Raman signals depends on the fourth power of the local electric field that is very high at the AuNP surface due to the plasmon resonance. This enhancement also originates, in addition, from electronic coupling between adsorbed molecules and the AuNP surface resulting from charge transfer between the AuNP metal surface and adsorbed molecules. Since the selective enhancement of SERS is correlated with polarization-dependant resonance bands, amplified electromagnetic fields at AuNP junctions contribute to SERS. Thus, in addition to the *elastically* scattered visible light by the AuNPs themselves that can be imaged using a dark-field optical microscope, the

AuNP surface provoke an *inelastic* SERS effect due to adsorbed molecules providing a Raman spectrum that leads to the identification of these molecules.<sup>26</sup> The two main strategies for SERS detection are (i) direct identification of Raman-active AuNP-adsorbed molecules and (ii) indirect detection of molecules incorporated into a biolabel. Interference from competing adsorbates can sometimes inhibit the

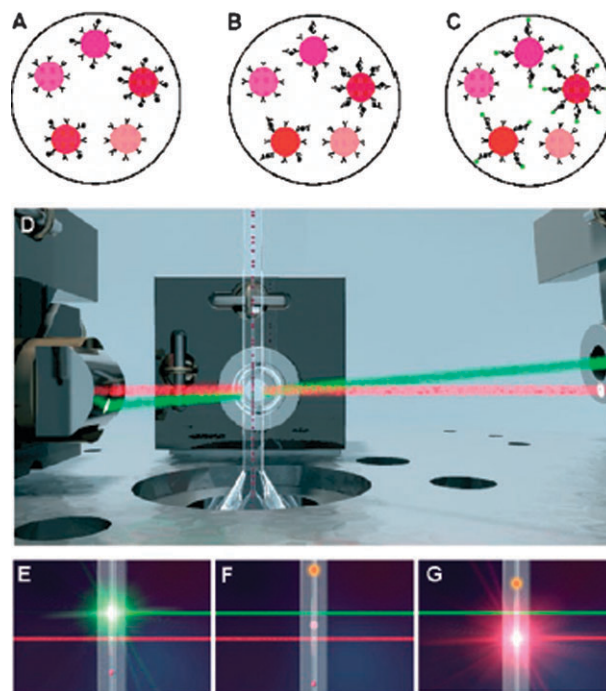


**Fig. 5** This series of images show how multiplexed assays are carried out with a suspension array. (A) The suspension array, composed of encoded microspheres conjugated to capture antibodies, is mixed with a sample containing different cytokines. (B) The cytokines are sandwiched between the capture antibodies and the corresponding biotinylated detector antibodies. (C) Bound detector antibodies are labeled with fluorescent reporter molecules. (D) A stream of individual microspheres flows through the sensing points of a cytometer. (E–G) Images of a single encoded microsphere with bound reporter molecules as it flows past (E) a green laser that excites the reporters and (G) a red laser that excites the code. (Courtesy of Luminex Corp.) Reprinted with permission of Wiley InterScience (ref. 44, Wilson's group).

detection of molecules in complex solutions. The plasmon band can also be tuned from the visible region for spherical AuNPs to the NIR by changing the size (redshift with larger size), shape (AuNRs and AuNSs), aggregation (inter-AuNP distance lower than AuNP size) and medium (increase of the refractive index). A number of studies have optimized the SERS of small AuNP-adsorbed molecules with non-spherical AuNPs, and on the biological side El-Sayed *et al.* have recently shown that oral cancer cells can align AuNRs that have been conjugated with anti-epidermal growth factor receptor antibodies on the cell surface, leading to a SERS fingerprint specific of the cancer cells.<sup>42</sup> The Halas group has discriminated between acidic cancer cells and healthy cells by monitoring changes in the Raman spectrum induced by pH changes over a suitable range with carboxy groups of a mercaptobenzoic acid layer on AuNSs that were active in the NIR region where blood and tissues are less absorbing.<sup>43</sup>

The Wilson group has recently reported the use of this SERS method as signatures in multiplexed detection, based on the fact that each spectrum is unique and composed of multiple bands that are much narrower than those of fluorescent dyes or quantum dots (Fig. 5).<sup>44</sup> Wilson has reviewed this field,<sup>45</sup> and a number of companies have marketed Raman detectors, such as Oxonica (Oxford, UK), with biotags that detect up to three respiratory viruses in the same sample (Fig. 6).<sup>46</sup>

A few SERS applications of AuNPs follow. Mammalian cells surfaces were imaged using SERS with nitrile-functionalized AuNPs. SERS hot sites correlate well with small aggregated AuNPs oriented preferentially in the

direction of incident laser polarization.<sup>47</sup> Spatially resolved probing and imaging of pH in live cells was demonstrated by SERS using 4-mercaptopbenzoic acid-AuNP aggregates (Fig. 7).<sup>48</sup> AuNPs conjugated with heterofunctional PEG ligands allowed facile conjugation of ScFv antibody as a targeting ligand for SERS detection of small tumors (0.03 cm<sup>3</sup>) at a penetration of 1–2 cm.<sup>49</sup> SERS imaging has been used for the targeting and highly sensitive imaging of specific cancer markers in live cells using core-shell Au-AgNPs conjugated with monoclonal antibodies (live HEK293 cells expressing PLC $\gamma$ 1) (Fig. 8).<sup>50</sup>

#### 4.4 Optical biosensors

Parak indicated that, whereas labeling and imaging above use AuNPs in a passive way, sensing involves an active role of the AuNPs.<sup>20</sup> The AuNP-distance dependence of the analyte detection (antigens, nucleic acids, aptamers, enzymatic reactions) using the plasmon resonance as well as size and refractive-index dependence have recently been comprehensively reviewed by Wilson.<sup>45</sup> Thus, only some representative and new examples of plasmon-related sensors are illustrated below. The dramatic influence of the inter-AuNP distance on the plasmon resonance, when this distance is reduced to less than the AuNP diameter, is indeed the crucial factor in the sensor applications of AuNPs. Thus, linking AuNPs with a biological analyte results in color change that makes the basis of sensing, a principle pioneered by Leuvering,<sup>51</sup> for which sensitivity is now improved using hyper-Raleigh scattering (HRS), a differential light-scattering spectroscopy (DLSS).<sup>52</sup>

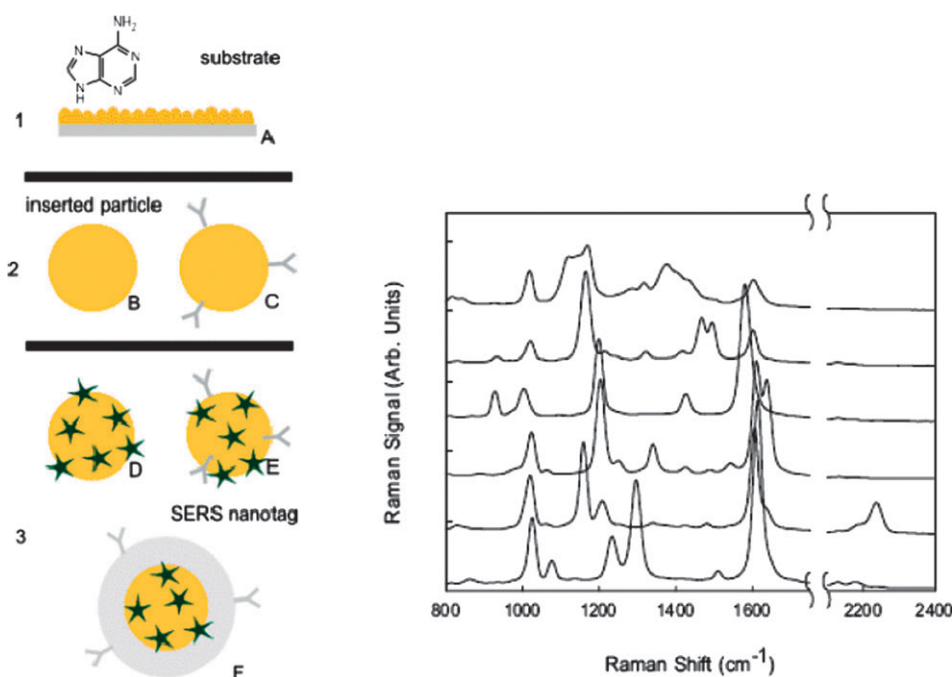


**Fig. 6** Architectures used in SERS experiments. (A) 2D substrate with adenine on the surface. (B) Bare particle. (C) Antibody-targeted particle. (D) Reporter labeled particle. (E) Targeted and labeled particle. (F) Targeted particle with encapsulated Raman label. A Represents the substrate approach, B and C are examples of the inserted particle approach while D, E, and F can all be thought of as SERS nanotags/Raman spectra of six different Nanoplex biotags. From top to bottom, the label molecules used were 4-[4-hydroxyphenylazo]pyridine, 4,4'-azopyridine, d8-4,4'-dipyridyl, bis(4-pyridyl)ethylene, bis(4-pyridyl)acetylene, 4,4'-dipyridyl. Reprinted with permission of Wiley InterScience (ref. 46, Freeman's group).

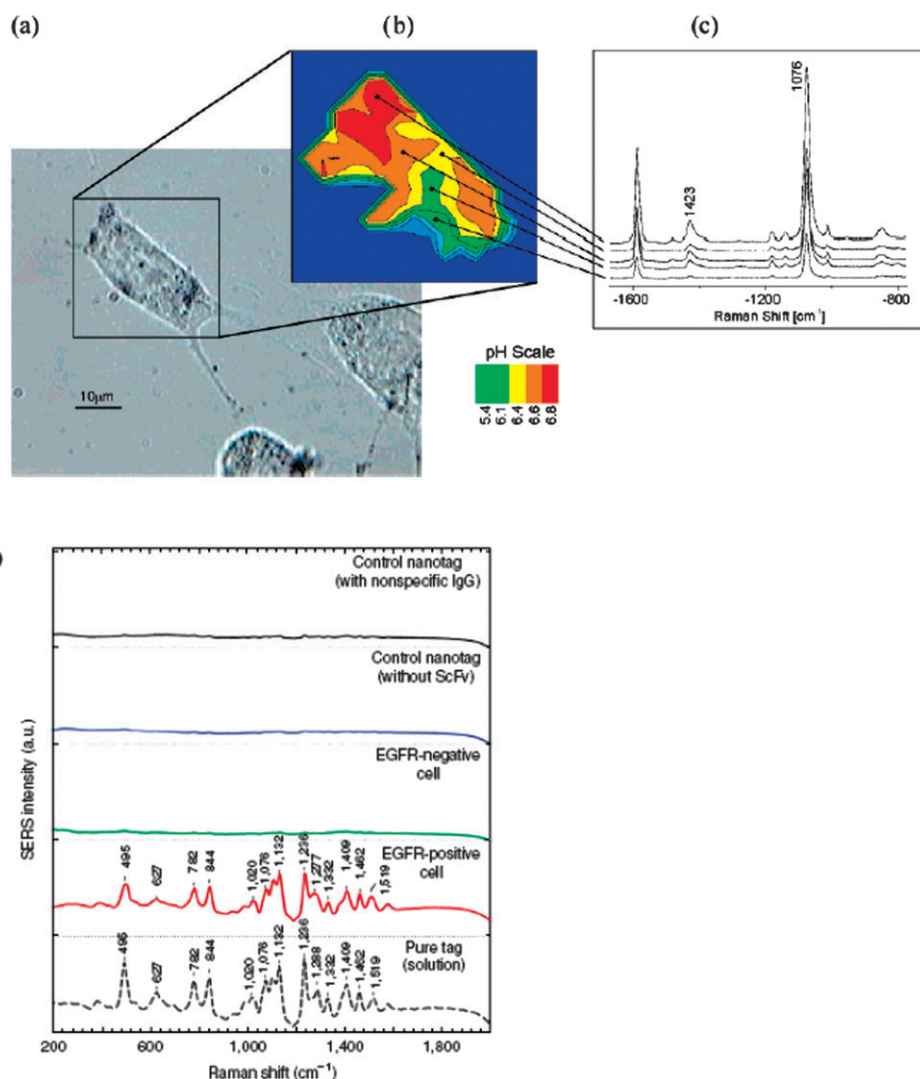


**Fig. 7** Probing and imaging pH values in individual live cells using a SERS nanosensor. (a) Photomicrograph of an NIH/3T3 cell after 4.5 h incubation with the pMBA gold nanosensor. Numerous gold nanoparticles have accumulated in the cell, enabling pH probing in different endosomes over the entire cell based on the SERS signature of pMBA. Lysosomal accumulations can be observed as black spots at the resolution of the light microscope. (b) pH map of the cell displayed as false color plot of the ratios of the SERS lines at 1423 and 1076 cm<sup>-1</sup>. The values given in the color scale bar determine the upper end value of each respective color. Scattering signals below a defined signal threshold (*i.e.*, where no SERS signals exist) appear in dark blue. (c) Typical SERS spectra collected in the endosomal compartments with different pH. The spectra were collected in 1 s each using 830 nm cw excitation (3 mW). Reprinted with permission of the American Chemical Society (ref. 48, Kneipp's group).

Mirkin and co-workers were the first to report colorimetric sensing of nucleic acids. Double-stranded DNA indeed link AuNPs with an inter-AuNP distance of only 0.34 nm causing a temperature-reversible red-to-purple color change. Each AuNP bears several oligonucleotides resulting in the formation of a network (aggregation) leading to the color change of the AuNPs to blue-violet, because of the reduced inter-AuNP distance.<sup>53</sup> Removing aliquots for spotting onto a C18 reverse-phase thin-layer chromatography plate as the temperature is increased results in a visual record of the color change that is known as the “*Northwestern spot test*”, the most well-known example of AuNP-based sensor. The addition of complementary target oligonucleotide strand by hybridization can be colorimetrically detected also leading to specific melting-temperature test for mismatched DNA.<sup>55–58</sup> Indeed,

even single DNA sequence mismatch results in a different disaggregation (melting) temperature provoking a color change.<sup>59</sup>

Studies of AuNP-DNA interactions have subsequently been pursued by several groups,<sup>60–63</sup> and quantitative detection of DNA sequences at very low concentration including detection of genetic mutations is now achievable using such a principle.<sup>59</sup> The Mirkin group has recently extended this method from specific detection of DNA sequences to a real-time screening assay for endonuclease activity.<sup>60</sup>

The Franco group has developed a non-cross-linking hybridization method also based on color changes, in which AuNP aggregation is induced by an increasing salt concentration. This method was used to detect eukaryotic gene expression (RNA) without need for retro-transcription

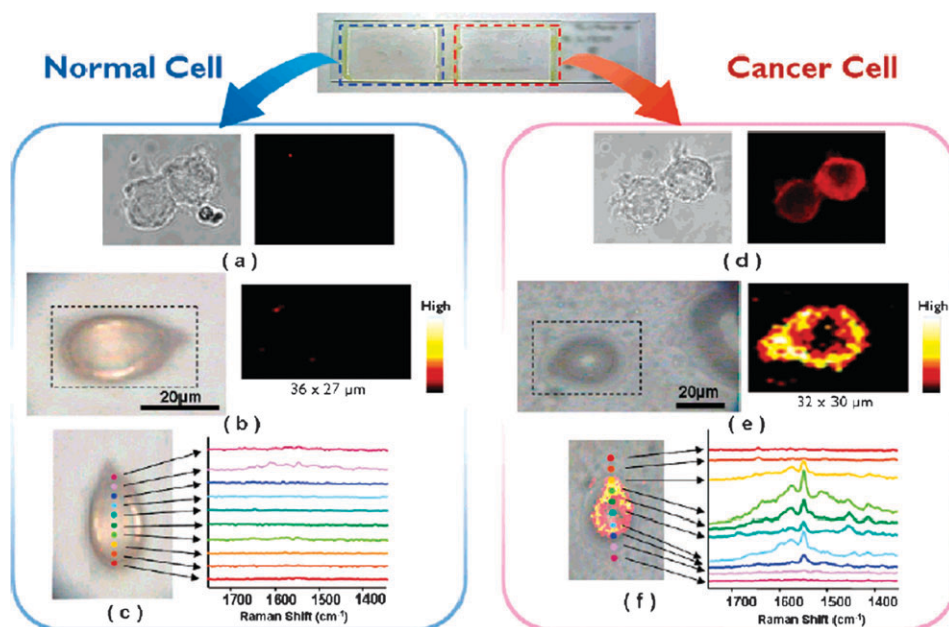


**Fig. 8** Fluorescence and SERS images of normal HEK293 cells and PLC $\gamma$ 1-expressing HEK293 cells. (a) QD-labeled fluorescence images of normal cells: (left) brightfield image, (right) fluorescence image. (b) SERS images of single normal cell: (left) brightfield image, (right) Raman mapping image of single normal cell based on the 1650  $\text{cm}^{-1}$  R6G peak. The cell area was scanned with an interval of 1  $\mu\text{m}$ . Intensities are scaled to the highest value in each area. (c) Overlay image of brightfield and Raman mapping for single normal cell. Colorful spots indicate the laser spots across the middle of the cell along the  $y$  axis. (d) QD-labeled fluorescence images of cancer cells: (left) brightfield image, (right) fluorescence image. (e) SERS images of single cancer cell: (left) brightfield image, (right) Raman mapping image of single cancer cell based on the 1650  $\text{cm}^{-1}$  R6G peak. The cell area was scanned with an interval of 1  $\mu\text{m}$ . Intensities are scaled to the highest value in each area. (f) Overlay image of brightfield and Raman mapping for single cancer cell. Colorful spots indicate the laser spots across the middle of the cell along the  $y$  axis. Reprinted with permission of the American Chemical Society (ref. 50, Choo's group).

or PCR amplification. It was possible to detect mRNA from 0.3  $\mu\text{g}$  of unamplified total RNA.<sup>61</sup> The detection of proteins and antibodies (anti-protein A, biotin and streptavidin and lectin) as well as molecules (adenosine, glucose) and metal ions (Pb, Hg, Cd, Li) has also been achieved using AuNPs in this way (Fig. 9).<sup>26,62</sup>

Although spherical AuNPs work well, non-spherical ones have also been used, the advantage being that the plasmon frequency can be finely adjusted with AuNRs and AuNSs. For instance, the Halas group has synthesized AuNSs with a 96-nm diameter and a 22-nm shell thickness to carry out distance-dependent immunoassays in dilute serum,<sup>63,64</sup> and the Murphy group has used biotin-avidin as a model system for optical detection of aggregated AuNRs (*i.e.* biotinylated AuNR aggregation upon addition of the protein streptavidin).<sup>26,65</sup> Other 3-D assemblies of AuNRs and AuN wires using DNA

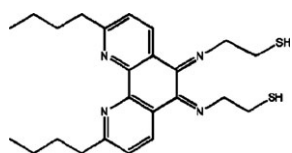


**Fig. 9** Chemical structure of the modified 1,10-phenanthroline ligand that binds to gold nanoparticles through the thiols, and to lithium ion through the chelating phenanthroline nitrogens. Two ligands are required to bind to one lithium ion in a tetrahedral fashion. Reprinted with permission of the Royal Society of Chemistry (ref. 26, Murphy's group).

are known.<sup>66–68</sup> Transducers have been set up to detect streptavidin concentration through the specific recognition with biotin-conjugated AuNPs. Polyelectrolyte functionalization provides a simple way to conjugate AuNPs with charged molecules such as biotin.<sup>69</sup> Chilkoti *et al.* have tracked scattering changes at 780 nm from a single AuNR to sense streptavidin in nanomolar concentration, using a dark-field microscope (Fig. 10 and 11).<sup>70</sup>

Willner and co-workers reported the first example of AuNP combination with thiolated aptamers (*i.e.* DNA-, RNA- or peptide-based sequences) thereby showing how thrombin could be detected upon aptamer-conjugated-AuNP linking.<sup>71</sup> PEG-15-nm-AuNPs covalently bound to F19 monoclonal antibodies *via* terminal PEG carboxylate group were used to label stroma tumor in resected pancreatic adenocarcinoma, and the tissues were imaged by darkfield microscopy at 560 nm.<sup>72</sup> Wilson has summarized the methods of detection that involve separation steps including microsphere assays and planar support.<sup>45</sup> Detection methods based on separation, must be used to improve sensitivity when naked eye detection is insufficient. Deposition of Ag onto the AuNPs upon Ag(I) reduction, called Ag enhancement was pioneered by Mirkin's group.<sup>73</sup> It allows imaging with unaided eye as the spot size after enhancement reaches 200 nm (a technique improved upon replacing Ag by Au).<sup>45</sup> Unamplified DNA and RNA target sequences can be detected in the presence of genomic DNA in this way, and CCD cameras and CD players have been used for recording such biosensing events.<sup>74</sup> The easiest

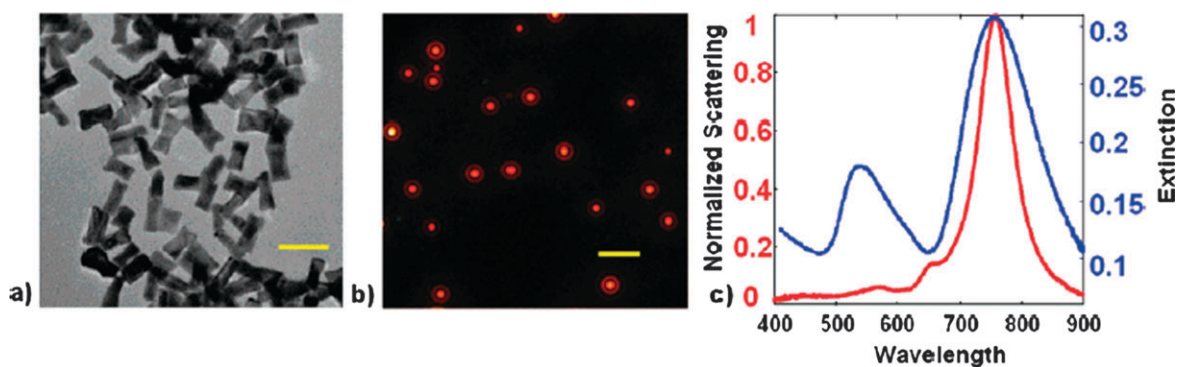


**Fig. 10** (a) TEM of gold nanorods used for biodetection experiments and (b) dark-field micrograph of gold nanorods immobilized on a glass substrate. (c) Scattering spectra of a single gold nanorod on a glass substrate (red) and the extinction spectrum of an ensemble of gold nanorods suspended in water (blue). Scale bar is 100 nm in (a) and 5  $\mu$ m in (b). Reprinted with permission of the American Chemical Society (ref. 70, Chilkoti's group).

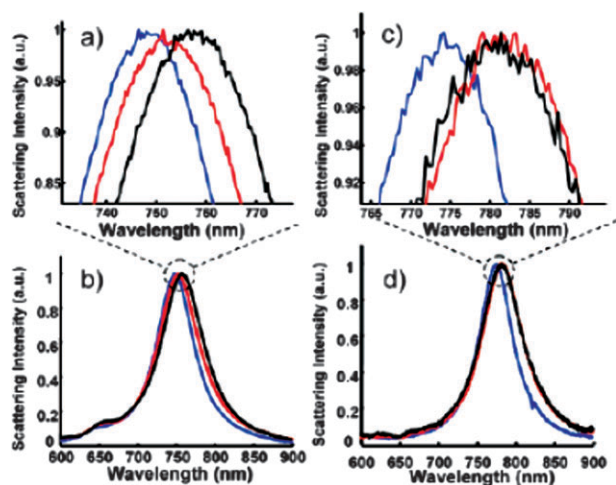


**Fig. 11** (a and b) Scattering spectra of a single gold nanorod after sequential incubation in EG3SH/MHA (blue), biotin (red), and 10 nM streptavidin (black). (c and d) Scattering spectra of a single gold nanorod in EG3SH/MHA (blue), biotin (red), and 100 nM streptavidin presaturated with free biotin (black). Reprinted with permission of the American Chemical Society (ref. 70, Chilkoti's group).

AuNP supports are 0.5- $\mu$ m polystyrene microspheres, but assays also use planar supports (glass, nitrocellulose, nylon<sup>45</sup> and thin films<sup>75</sup>). Magnetic microspheres that facilitate separation of bound AuNPs have also been reported.<sup>76</sup> Other separation methods involve lateral flow devices for immunoassays, nucleic acid flow devices, flow-through devices, blots and arrays, silver-enhanced arrays, "biobarcode" (marker) assays, electrical detection, SERS and fingerprint detection.<sup>45</sup>

#### 4.5 Fluorescence

Fluorescence of AuNPs includes fluorescence spectrometry, fluorescence correlation spectroscopy (FCS) and fluorescence microscopy. Especially, the fluorescence of AuNPs possesses the excellent behavior of antiphotobleaching under strong light illumination. Despite low quantum yields, AuNPs exhibit strong native fluorescence under relatively high excitation power. The fluorescence of AuNPs could be characterized by fluorescence imaging and FCS at the single-particle level. A new fluorescence method for cell imaging involves, after

cells stained with AuNPs are illuminated with strong light, the fluorescence of AuNPs on cell membrane or inside cells that can be collected for cell imaging.<sup>77</sup>

Fluorescence Resonance Energy Transfer (FRET) is a spectroscopic technique whereby the excitation energy of the donor is transferred to the acceptor *via* an induced-dipole,

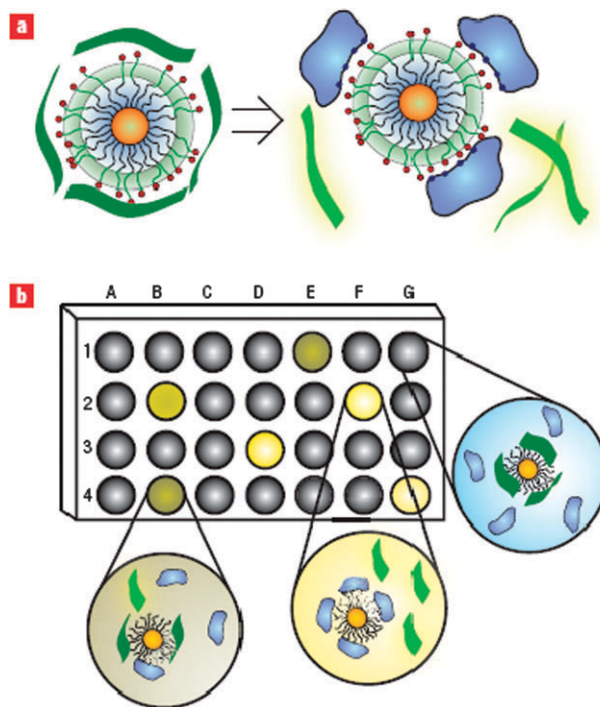


**Fig. 12** Fluorophore displacement protein sensor array. (a) Displacement of quenched fluorescent polymer (dark green strips, fluorescence off; light green strips, fluorescence on) by protein analyte (in blue) with concomitant restoration of fluorescence. The particle monolayers feature a hydrophobic core for stability, an oligo(ethylene glycol) layer for biocompatibility, and surface charged residues for interaction with proteins. (b) Fluorescence pattern generation through differential release of fluorescent polymers from gold nanoparticles. The wells on the microplate contain different nanoparticle-polymer conjugates, and the addition of protein analytes produces a fingerprint for a given protein. Reprinted with permission of the Nature Publishing Group (ref. 80, Rotello's group).

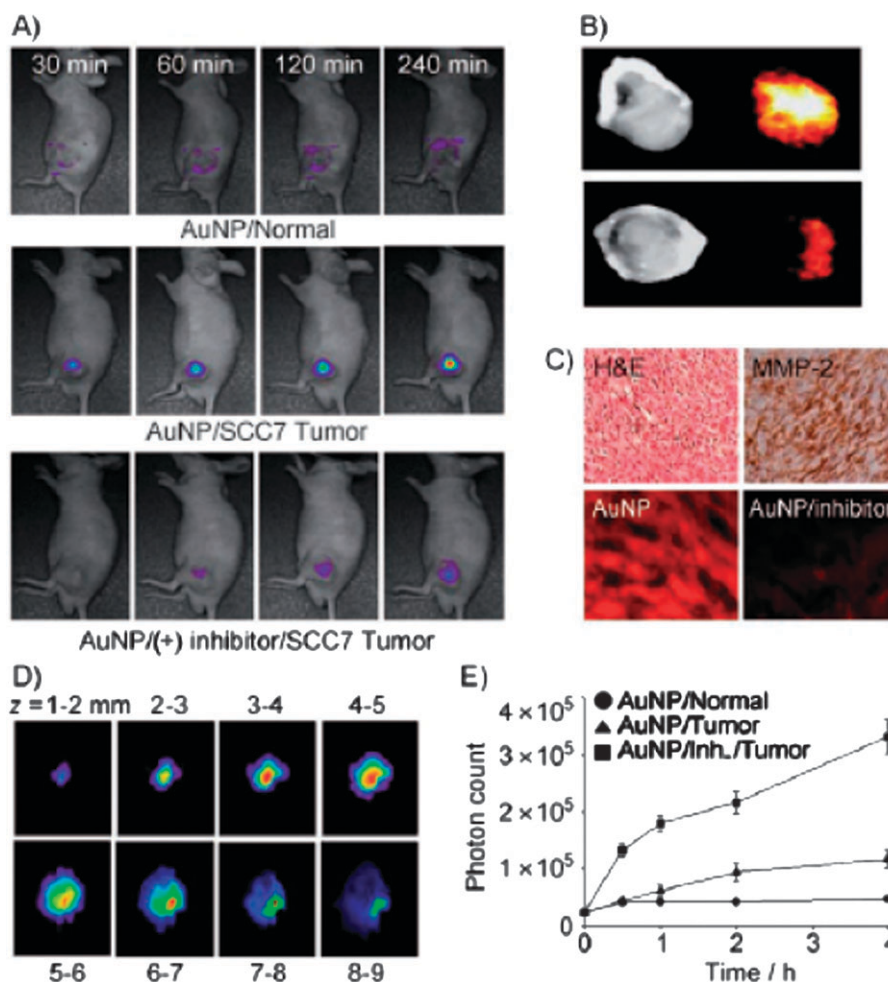


**Fig. 13** (A) NIRF tomographic images of normal and subcutaneous-SCC7-tumor-bearing mice after injection of the AuNP probe with and without inhibitor (blue: low intensity, red: high intensity). (B) NIRF images of excised AuNP-probe-treated SCC7 tumors with and without MMP-2 inhibitor. (C) Immunohistology results for SCC7 tumors with MMP-2. H&E = Hematoxylin/eosin stain; lower row: NIRF microscopy of SCC7 tumors containing AuNP probes without and with inhibitor. (D) 2D slices of the image from (A) reconstructed in the *z* direction (blue: low concentration, red: high concentration). (E) Quantitative image analysis performed by counting the total number of photons in the tumors as a function of time. Reprinted with permission of Wiley InterScience (ref. 81, Ahn's group).

induced dipole interaction. The efficiency of energy transfer  $E$  is given by  $1/[1 + (R/R_0)^6]$  where  $R$  is the distance between the donor and the acceptor and  $R_0$  is the distance at which 50% of the energy is transferred; thus small distance changes result in sizeable change in  $E$ . With AuNPs, at small distance ( $<1$  nm), radiative rate enhancement is observed; at 2–3 nm, energy transfer dominates, and at large distances ( $>50$  nm), fluorescence oscillations take precedence. AuNP-based FRET monitors DNA hybridization and DNA cleavage by nucleobases. For instance, after hybridization, by varying the DNA length, the separation distance between AuNP and Cy3 dye was systematically varied between 3 and 100 nm, and 50% quenching efficiency was observed even at 25 nm separation.<sup>78</sup> Fluorescent dyes and quantum dots are quenched by close proximity of AuNPs, even at distances larger than 2 nm. Quenching effects have even been shown to operate over much larger distances than the Förster resonance quenching transfer distance between dyes.<sup>79</sup> Therefore, increase of fluorescence is observed upon hybridization to a complementary nucleic acid sequence, because the fluorescent dye or quantum dot and the

quencher are forced apart. In this way, large molecules such as proteins can be sensed, and Rotello *et al.* have applied this principle using a fluorescent polymer to decode the response produced by nanomolar concentrations of proteins in unknown samples based on selective AuNP-protein affinities (Fig. 12).<sup>80</sup> For instance, 20-nm AuNPs stabilized by Cy5.5-Gly-Po-Leu-Gly-Val-Arg-Gly-Cys-(amide) showing selectivity for a matrix metalloprotease served as fluorescent imaging probe for *in vivo* drug screening and protease activity (Fig. 13).<sup>81</sup>

#### 4.6 Electrochemical biosensors

AuNPs are useful in electrochemical bioassays, in particular to connect enzymes to electrode surfaces, mediate electrochemical reactions as redox catalysts and amplify recognition signals for biological processes.<sup>82</sup> Their first use as labels for immunosensors was reported by the group of Degrand and Limoges,<sup>83</sup> which was followed by hundred of electrochemical bioassay articles including excellent reviews.<sup>84–86</sup> The two

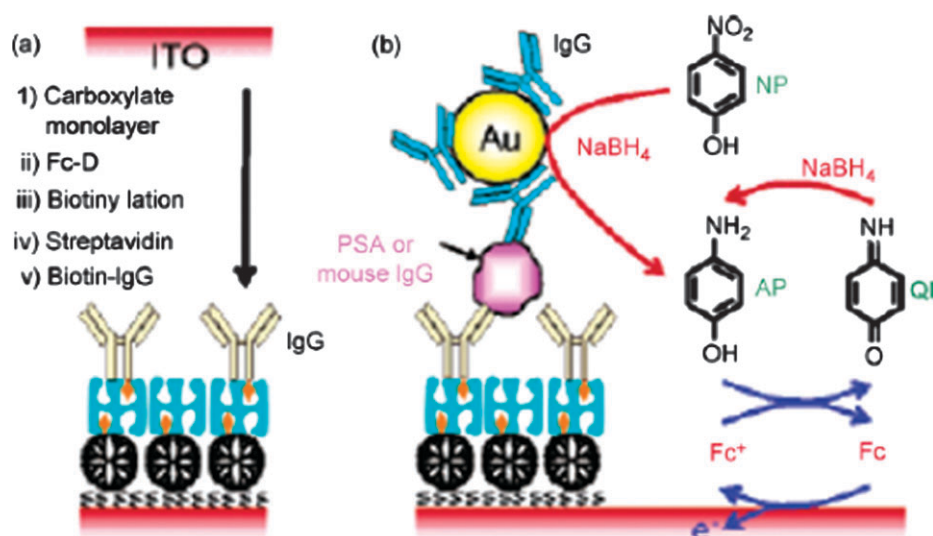


**Fig. 14** (a) Schematic representation of the preparation of an immunosensing layer. (b) Schematic view of electrochemical detection of mouse IgG or prostate specific antigen. Reprinted with permission of the American Chemical Society (ref. 85, Wang's group).

main research areas are AuNP nanoelectrodes for bioassays and AuNPs as biomolecular tracers, and in both of them applications are found in enzymatic biosensing, genosensing and immunosensing.

As a representative example, AuNPs are used as wires connecting electrode surfaces to the redox center of enzymes. Fixation of the AuNPs onto the electrode surface provides a microenvironment comparable to that of redox proteins and more protein freedom for orientation. In this way, the insulation by the protein shell is reduced, and electron transfer can occur through the conducting tunnels of the AuNPs (Fig. 14).<sup>85</sup> Thus, AuNPs attached to enzymes such as, typically, glucose oxidase (GO), serve as nanoelectrodes so that the turnover rate of electrons transferred *via* AuNPs to the electrode surface reaches about 5000 which is seven times higher than the turnover rate of electrons from the active site of GO to O<sub>2</sub>.<sup>87–89</sup> As an amperometric and potentiometric immunosensor example, multilayer films of negatively charged AuNPs/positively charged tris(2,2'-bipyridyl)cobalt(III) were assembled on a Pt electrode surface covered with a layer of plasma-polymerized Nafion film for hepatitis B surface antigen determination.<sup>90–92</sup>

For genosensor applications (DNA electrochemical sensing), AuNPs modified with thiol-functionalized oligonucleotides were submitted to hybridization of the target DNA sequence. This type of assay relies on the release of AuNPs by oxidative metal dissolution and indirect determination of the HBr solubilized Au(III) ions by anodic stripping voltammetry.<sup>93,94</sup> Subsequently, methods based on the direct electrochemical detection of the AuNP tag were developed in order to avoid the high toxicity of the HBr/Br<sub>2</sub> oxidant.<sup>95,96</sup> A signal amplification strategy consists in attaching ferrocenyl-hexanethiol or electrogenerated chemiluminescence (ECL) indicator to the AuNP label. AuNP-streptavidin conjugate to which 6-ferrocenylhexanethiol was bound were attached onto a biotinylated DNA detection probe of a sandwich DNA complex. A detection limit of  $5 \times 10^{-12}$  mol L<sup>-1</sup> for target DNA was reached.<sup>97</sup> The use of AuNPs for

“fingerprint” detection involves immersion of a substrate in AuNPs at low pH provoking electrostatic binding to the print that is enhanced by catalytic deposition of Ag or better, Au.<sup>98</sup>

AuNPs bearing alkylthiolate ligands terminated with redox centers<sup>99,100</sup> proved to be useful for the redox recognition, sensing and titration of ATP<sup>2-</sup>,<sup>101,102</sup> an electrochemical method based on the shift of redox potential of the redox system attached to the ATP recognition site (ferrocenylsilyl or amido-Fe<sub>4</sub> cluster).<sup>103</sup> AuNP-centered dendrimers are most useful for this type of sensing, because the positive dendritic effect (increase of potential shift as the dendrimer generation increases) facilitates sensing.<sup>104</sup> Large dendritic AuNPs adsorb so strongly on Pt electrodes for sensing using the AuNP-dendrimer-modified electrode that the modified electrodes are robust enough to be washed for further re-use.<sup>104</sup>

## 5. Clinical diagnostics

### 5.1 General

AuNPs have been used as radioactive labels *in vivo* since the 1950s, and immuno-AuNPs conjugated to antibodies have been used since the 1980s for biological staining in electron microscopy. They present several advantages in biodiagnostic over quantum dots and organic dyes: (i) much reduced or no toxicity (*vide infra*), (ii) much better contrast agents for imaging (compare with organic dyes that suffer from rapid photobleaching), (iii) surface-enhanced and distance- and refractive index-dependent spectroscopic properties. In their excellent micro-review article, Baptista *et al.* distinguish three approaches for biodiagnostics based on AuNPs: (i) inter-AuNP distance dependent colorimetric sensing for specific DNA hybridization for the detection of specific nucleic acid sequences in biological samples (the most developed approach), (ii) surface-functionalized AuNPs providing highly selective nanoprobe, and (iii) electrochemical-based methods for signal enhancement.<sup>61</sup> The bases of these methods are detailed in the preceding sections. Here, we are essentially emphasizing clinical diagnosis applications.

Among the clinical diagnosis methods involving AuNPs immunoassays, promising applications are found in signal enhancement of the standard enzyme-linked immunosorbent assays (ELISAs) such as immunochromatographic test strips where both the primary and secondary antibodies are conjugated with the AuNPs.<sup>105</sup> The detection of the chorionic gonadotropin hormone reaches  $1 \text{ pg mL}^{-1}$  using this set-up. Other sensors are based on AuNP-functionalized fiber-optic evanescent wave<sup>106</sup> or AuNP-functionalized Cy5-antibody as the fluorescence probe which could replace the standard ELISA assay, because they do not require a secondary antibody and offer increased sensitivity.<sup>107</sup>

Chemiluminescent analysis of antibodies, such as anti-IgG to determine IgG content in human plasma, is optimized with irregular-shaped AuNPs that are more active than spherical AuNPs.<sup>108</sup> Hirsch *et al.* have reported a rapid whole-blood immunoassay using AuNSs capable of detecting sub-nanogram-per-milliliter quantities of various analytes upon aggregation of antibody-AuNS conjugates including successful detection of immunoglobulins in saline serum and whole blood. The simplicity of this assay also makes it superior to conventional ELISAs, because it requires less technical proficiency than ELISAs.<sup>109</sup>

The use of AuNPs is very promising in the field of immunosensors based on metal-enhanced fluorescence.<sup>110</sup> As recent examples of the use of electrochemical approaches based on the derivatization of electrodes with AuNPs, let us mention the label-free detection of the carcinoembryonic antigen (CEA).<sup>111,112</sup> A sensitivity-enhanced immunosensor based on the SPR was developed for the detection of by AuNR-antibody complex.<sup>113</sup> The pathogen *Escherichia coli* O157:H7 was rapidly detected on a piezoelectric oligonucleotide-AuNP-based biosensor.<sup>114</sup> Below, we summarize AuNP diagnostic for main diseases.

## 5.2 Cancer

Cancer diagnosis/detection based on the imaging of micro-anatomical features of diseased tissues uses OCT and RCM methods (*vide supra*). Cancer biomarkers and optical contrast agents provide excellent signal sources from cancer tissues. The intense scattering of large AuNPs makes them promising probes for cancer detection based on imaging. Immunotargeting of antibody-AuNPs label cancer cells by conjugating them with antigens overexpressed in cancer cells. For instance, cervical epithelial cancer cells (SiHa cells) that overexpress the transmembrane glycoprotein, epithelial growth factor receptor (EGFR), were imaged by immunotargeted AuNPs. AuNP scattering was strong enough to allow the use of even a red laser pointer, a resource-poor setting, instead of a scanning laser to image the cancer cells.<sup>115</sup>

Besides antibodies and some viruses, some biomolecules such as in particular folate are avidly taken up by cancer cells, which allows their selective targeting (Fig. 15).<sup>116</sup> El-Sayed *et al.* demonstrated the use of dark-field microscopy, an extremely simple and inexpensive technique, for the successful selective detection of cancerous cells. Thus, 35-nm AuNPs conjugated with anti-EGFR antibodies immunotargeted to two malignant epithelial cell lines were selected for optimal intense surface plasmon scattering using a white-light source

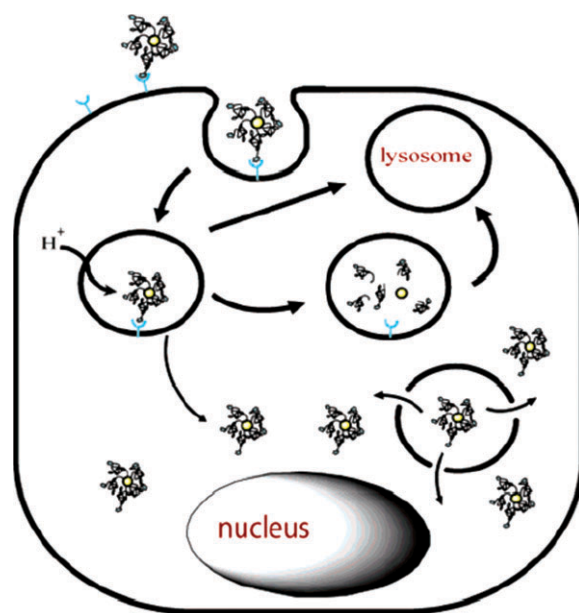


**Fig. 15** Conceptual diagram of folate receptor-mediated binding, internalization, endosomal acidification, intracellular trafficking, and endosomal escape of F-PEG1500-T:AuNP by folate receptor-positive cells. Reprinted with permission of the American Chemical Society (ref. 116, Andres's group).

from a conventional microscope resulting in a colored AuNP image with dark background.<sup>117</sup> Extension to other optical imaging techniques such as photo-acoustic tomography, multiphoton plasmon resonance microscopy, optical coherence microscopy and third-harmonic microscopy for cancer imaging is promising.<sup>118</sup>

The nanoprobe method has been used by the Franco group to detect single nucleotide polymorphisms (SNPs) and mutations due to diseases such as cancer.<sup>119,120</sup> Recently, a colorimetric assay was reported for the direct detection of cancer cells by using aptamer-conjugated AuNPs. It was shown that the AuNP-aptamers could be assembled on a cell membrane surface for spectral changes, providing a direct visualization of cancer cells. The assay was also demonstrated on two different cell types that had cell-SELEX aptamers selected for them, indicating possible extension for any cell type. This could include colorimetric assays for various cancers or other diseases. The cell-SELEX aptamers have been generated for leukemia and lymphoma, lung cancer and liver cancer, suggesting that the assays could work out for the detection of these diseases.<sup>121</sup> Purine-9- $\beta$ -D-ribofuranoside were found to substantially enhance the anti-proliferative effect against K-562 leukemia cells, due to enhanced intracellular transport followed by the subsequent release in lysosomes (Fig. 16).<sup>122</sup> AuNPs covalently conjugated with PEG and monoclonal antibody Herceptin, that enables recognition of breast cancer cells expressing specific tumor associated antigens, were shown to be stable and active *in vitro* in the presence of blood and *in vivo* in nude mice model for breast cancer.<sup>123</sup>

Many articles deal with both diagnostic and therapy, especially those dealing with the SPB-based photothermal effects, thus the reader is also referred to the other sections of this review concerning cancer.

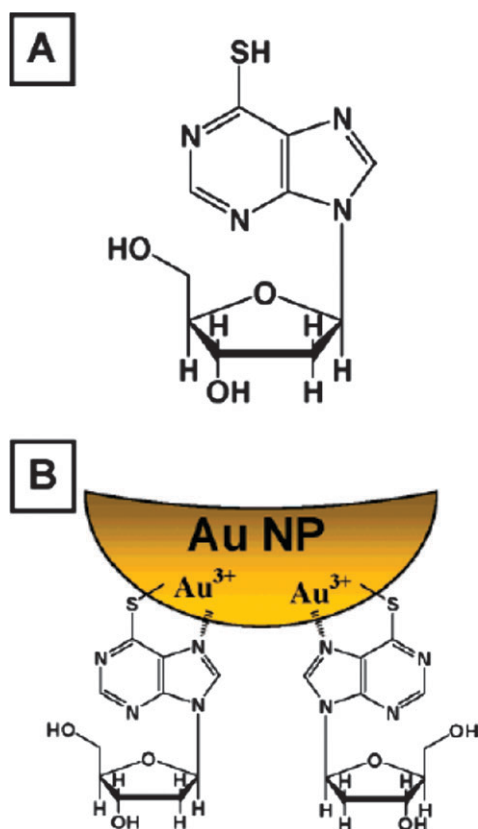


**Fig. 16** Gold nanoparticles stabilized with 6-mercaptopurine-9-β-D-ribofuranoside. (A) Chemical formula of 6-MPR. (B) Schematic of 6-MPR stabilization of AuNPs. Simple geometrical calculations based on the available surface atoms and/or geometry of the (6-MPR) moiety indicates that there might be 100–350 molecules of 6-MPR on the surfaces of the AuNPs. Reprinted with permission of the American Chemical Society (ref. 122, Kotov's group).

### 5.3 Alzheimer

Pioneering work toward an assay of Alzheimer diseases using AuNPs has been firstly reported by Van Duyne's group where a nanoscale optical biosensor based on LSPR spectroscopy has been described to monitor the interaction between the antigen, amyloid derived diffusible ligands (ADDLs), and specific anti-ADDL antibodies.<sup>124,125</sup> The Mirkin traditional method consisting in AuNP-nanoprobe cross-linking known for protein detection in attomolar sensitivity was successfully used for measuring the concentration of amyloid-β-derived diffusible ligands, a potential Alzheimer disease marker present at extremely low concentration ( $<1 \text{ pmol L}^{-1}$ ) in the cerebrospinal fluid of affected individuals.<sup>126</sup>

### 5.4 HIV

Multivalent AuNPs were found to inhibit HIV fusion. Therefore, 2-nm AuNP-mercaptopbenzoic acid were conjugated to SDC-1721, a derivative of TAK-779, a known CCR5 antagonist that serves as the main entry co-receptor for most commonly transmitted strains of HIV-1. In this way, TAK-779 inhibited HIV-1 replication with an  $\text{IC}_{50}$  of 10 nM (Fig. 17).<sup>127</sup> A highly sensitive screening assay based on electrochemical impedance spectroscopy (EIS) has been

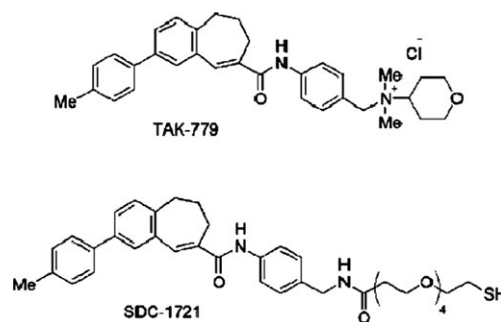


**Fig. 17** TAK-779 and SDC-1721. Reprinted with permission of the American Chemical Society (ref. 127, Feldheim's group).

developed for the detection of HIV-1 protease using a thiol-terminated ferrocenyl-pepstatin conjugate was therefore attached to a single-wall carbon nanotube-AuNP modified electrode.<sup>128</sup>

### 5.5 Hepatitis B

Successfully prepared AuNPs-Hepatitis B virus (HBV) DNA gene probes could be used to detect HBV DNA directly. The detection-visualized fluorescence-based method is highly sensitive, simple, low cost and could potentially apply to multi-gene detection chips.<sup>129</sup>

### 5.6 Tuberculosis

A successful application of the AuNP-nanoprobe colorimetric method to clinical diagnosis reported by Baptista *et al.* was the sensitive detection in clinical samples of *Mycobacterium tuberculosis*, the human tuberculosis etiologic agent.<sup>130</sup> A specific oligonucleotide [5'-thiol-GGACGTGGAGGC-GATC-3'] derived from the *M. tuberculosis* RNA polymerase β-sub-unit gene sequence, suitable for mycobacteria identification, was used. At high NaCl concentration, nanoprobe aggregation in the absence of a complementary DNA sequence turns the solution purple. In the event of specific probe hybridization to a complementary sequence (*i.e.* DNA from *M. tuberculosis*), no nanoprobe aggregation occurs, and the solution remains red.<sup>130</sup>

### 5.7 Diabetes

Diabetes was characterized as a multifactorial disease using the AuNP-nanoprobe method mentioned above and involving the capture of the analyte with a magnetic particle featuring recognition elements followed by binding of a AuNP with a second recognition agent and marker DNA strands for cancer detection.<sup>130</sup>

## 6. Therapy

### 6.1 Photothermal cancer therapy

Conventional treatments of most cancers are surgical removal that is limited to large, accessible tumors, chemotherapy that suffers from dramatic side effects, and radiotherapy that is also invasive to healthy tissues along the radiation path. On the other hand, laser hyperthermia (photothermal therapy) that uses optical heating for tumor ablation is a mild solution that

avoids all these drawbacks. Organic photoabsorbers such as *Indocyanine green* and inorganic ones such as iron oxide have been used for photothermal tumor ablation but suffer respectively from small cross section requiring high irradiation energy and the need of iron oxide in high quantities (up to 10% weight) that is more or less toxic. The advantages of AuNPs are that they have high absorption cross sections requiring only minimal irradiation energy and are considered as non-toxic (*vide infra*). Irradiation of the SPR of AuNPs is followed by fast conversion of light into heat (about 1 ps).<sup>131–135</sup> Relatively small AuNPs (*e.g.* 10–30 nm) are delivered more easily to cancer cells using various methods (physiological transportation, conjugation with antibodies, *etc.*) than larger AuNPs.<sup>136</sup> After delivery, these AuNPs are self-assembled into larger clusters of closely located AuNPs directly within cells, resulting in laser-induced bubble formation that are more effective for cell killing and SPR shift from the visible region to the 700–1000 nm NIR region.<sup>137</sup>

AuNPs of various shapes absorb light in a broad spectrum range from near UV to NIR, but the NIR region is especially crucial in order to penetrate inside living tissues unlike visible light. The depth of light penetration can reach a few centimetres in the “biological window” (650–900 nm), a region ideal for the SPR absorption of AuNSs, AuNRs and Au nanocages. Thus, localized photothermal destruction of SK-BR-3 cancer cells was demonstrated by the Halas group *in vitro* and *in vivo* using thiolated-PEG-passivated AuNSs (passivation avoids aggregation in saline solution) with a 110 nm-diameter core and a 10 nm-thick shell resulting in a peak absorbance at 820 nm designed to match the emission wavelength of the diode laser. *In vitro*, silver staining revealed

that the protein-adsorbent AuNS surface promoted binding to the AuNS surface. *In vivo*, the temperature increase upon AuNS NIR irradiation was of  $37.4 \pm 6.6$  °C at a depth of 2.5 mm beneath the dermal surface on 5 min exposure, which is well above the temperature at which irreversible tissue damage occurs (40 °C) with laser dosage 10 to 25 times less than those used with *Indocyanine green* dye. Maximal depth of treatment was 6 mm, but could reach 1 cm or even more in related studies.<sup>131</sup> In order to explain these very positive therapy results, it appears that thiolated PEG ligands, that are biocompatible, mask the AuNPs from the immune system and inhibit aggregation. These PEG ligands also facilitate accumulation of the AuNSs at the tumor site due to the highly permeable vascular network in neoplastic tumors, referred to as the so-called “enhanced permeability and retention (EPR) effect”.<sup>138</sup> Indeed, PEGs are currently used as carriers of anticancer drugs, and the efficiency of this means must be related to this EPR effect. In addition, selectively targeting of AuNPs to biomarkers on cancer cells appears as a very promising technique of cancer therapy.<sup>139,140</sup> Thus, using AuNSs conjugated with antibodies to HER2, a protein overexpressed in breast cancer cells, the Halas group photodamaged breast cancer cells *in vitro* using NIR laser phototherapy.<sup>133</sup>

The El-Sayed group used immunotargeted 40-nm AuNPs with two oral squamous cancer cell lines, HOC and HSC, that overexpress EGFR proteins. For this purpose, they used the 514-nm excitation of a common laser with the spherical AuNPs whose plasmon band had its maximum at 530 nm. These cancerous cells underwent photodamage *in vitro* within 4 min at laser energies of 19- and 25 W cm<sup>-2</sup> unlike AuNP-free

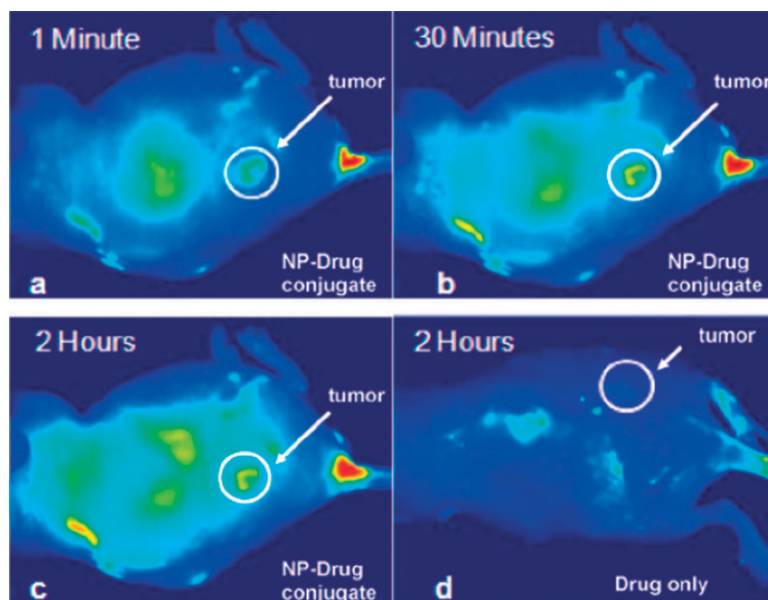


**Fig. 18** Fluorescence images of a tumor-bearing mouse after being injected with AuNP-Pc4 conjugates in normal saline (0.9% NaCl, pH 7.2), (a) 1 min, (b) 30 min, and (c) 120 min after intravenous tail injection. Any bright signal is due to Pc4 fluorescence, without which no fluorescence signals were detected from the mouse. (To reduce autofluorescence, the animal was fed a special diet for more than 2 weeks before the experiment.) Unprecedented delivery efficiency and accumulation rate of the drug in the tumor are monitored *via* the fluorescence increase in the tumor area (white circle). For comparison, a mouse that got only a Pc4 formulation without the AuNP vector injected is shown in panel (d). No circulation of the drug in the body or into the tumor was detectable 2 h after injection without the AuNP as drug vector. Reprinted with permission of the American Chemical Society (ref. 149, Burda's group).

cells. AuNRs with a strong longitudinal absorption in the NIR region around 800 nm were used to observe malignant HOC and HSC cells labeled with the AuNR bioconjugate, upon AuNR red scattering in dark-field optical microscopy. The over expression of EGFR on the cell cytoplasmic membrane for various tumors was used for the selective delivery of anti-EGFR biconjugates in high concentrations to cancer cells for phototherapy.<sup>141</sup> Excitation of AuNRs passivated by phosphatidylcholine using a pulsed Nd-YAG laser provoked cell death,<sup>142</sup> and excitation of AuNRs conjugated to folate using a CW Ti:sapphire laser was used for hyperthermia of KB oral cancer.<sup>143</sup>

Prospects for AuNRs in diagnostic and therapeutic applications have been reviewed.<sup>144</sup> AuNSs were also efficiently used *in vivo* with a subcutaneous prostate cancer (PC-3 cells) model whereby histological analysis of the tumor following direct tumor injection of AuNPs revealed even distribution throughout the tumor.<sup>145</sup> AuNSs conjugated to dextran afforded both photonic-based imaging and therapy of macrophage cells *in vitro*, which should prove useful for diseases such as atherosclerosis and in-stent restenosis.<sup>146</sup>

Hollow dendrite-shaped  $\text{Au}_{0.3}\text{Ag}_{0.7}$  NPs were used as NIR photothermal absorbers for destroying A549 lung cancer cells with laser powers required for cell damage significantly reduced relative to those used for AuNRs (Fig. 18).<sup>147</sup> 110-nm AuNSs with 10-nm shell thickness were used for prostate cancer ablation (PC-3 cells) using a 810-nm NIR laser with a 200-nm laser fiber and an energy setting of  $4 \text{ W cm}^{-2}$ , and resulted in 98% tumor necrosis.<sup>148</sup>

Phototherapies that do not use the AuNP SPB have also been reported. Photodynamic therapy using a PEG-5-nm-AuNP-Si-phthalocyanine conjugate generates singlet oxygen, very efficiently inducing apoptosis or necrosis directly in tumor-bearing mice as shown by fluorescence images. In this case, a crucial point is that the Au-PEG vector preferentially accumulates in tumor sites through the leaky tumor vasculature ("enhanced permeability and retention", EPR effect).<sup>149</sup>

## 6.2 Radiofrequency therapy

Radiofrequency (RF) current, with a frequency between 10 kHz and 900 MHz has been applied for medical purposes for nearly a century with limited use due to thermal injury, but has been proposed in the 1990s as effective for destroying liver tumors. Limitations, however, included the requirement for invasive needle placement, accuracy of image guidance, tumor size, and collateral damage to non-tumorous liver parenchyma and adjacent structures, the occurrence of learning curves and relatively high local tumor recurrence. Thus a non-invasive technique has very recently been reported for tumor ablation using a variable power (0–2 kW) RF signal (13.56 MHz) by direct injection of citrate-AuNPs into the tumor to focus the radiowave for selective heating both *in vitro* and *in vivo* (rat exposure at 35 W).<sup>150</sup> Human cell lines were also exposed to a 13.56 MHz RF field, and the resulting induced heat was lethal to these cancer cells bearing AuNPs *in vitro*.<sup>151</sup>

## 6.3 Angiogenesis therapy

Angiogenesis is the formation of new blood vessels from existing ones, and "abnormal" angiogenesis was shown to play an important role in the growth and spread of cancer, due to the feed of cancer cells by the new blood vessels with oxygen and nutrients. Mukherjee *et al.* discovered that AuNPs inhibit angiogenesis and recently published a review article on this subject.<sup>152</sup> The authors showed that addition of AuNPs profoundly inhibited phosphorylation of the proteins responsible for angiogenesis in a dose-dependent manner, almost complete inhibition being observed at concentrations of 335–670 nM. It was suggested that the responsible inhibition mechanism involves AuNPs direct binding to heparin-binding growth factors presumably through cysteine residues of the heparin-binding domain (Fig. 19).<sup>152</sup>

## 6.4 Rheumatoid arthritis therapy

AuNPs have been used in the treatment of rheumatoid arthritis for a very long time, and medical treatment dates

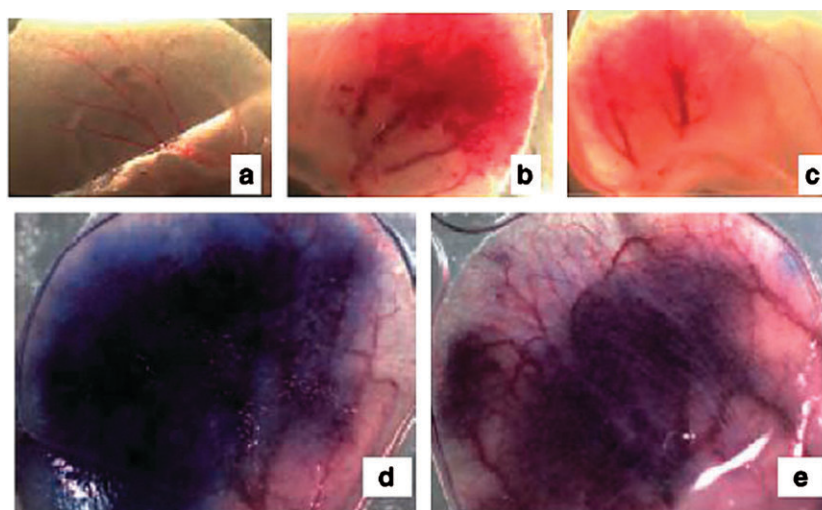


**Fig. 19** Effect of nanogold on angiogenesis *in vivo* in the ears of nude mice. Gross appearance of angiogenesis 7 days after injection of nanogold only (a), Ad-VEGF only (b), nanogold and Ad-VEGF (c). Effect of nanogold on permeability, Ad-VEGF only (d), nanogold and Ad-VEGF (e). Reprinted with permission of the American Association for Cancer Research (ref. 152, Mukherjee's group).

from the 1920s. Recently, it was shown that 13-nm AuNPs prepared by the citrate reduction method inhibited proliferation and migration of the protein responsible for angiogenesis. Angiogenesis plays a key role in the formation and maintenance of rheumatoid arthritis. Furthermore, animal testing by intradermal injection of these AuNPs for 7 and 10 days resulted in a significant reduction of joint inflammation, and immunohistochemical staining revealed a significant decrease in macrophage infiltration into the synovium of rats. This is important, because rheumatoid arthritis is still currently essentially incurable. Photoacoustic tomography of joints aided by an Etanercept-conjugated AuNR contrast agent was shown to visualize the AuNR-drug conjugate down to 1 pM in phantoms or 10 pM in biological tissues.<sup>153</sup>

### 6.5 Anti-bacterial therapy

Strong laser-induced overheating effects accompanied by the bubble-formation phenomena around clustered AuNPs cause bacterial damage, and this nanotechnology was used for selective killing of the Gram-positive *Staphylococcus aureus* by targeting bacteria surface using 10-, 20- and 40-nm AuNPs conjugated with anti-protein A antibodies.<sup>154</sup>

### 6.6 Drug vectorization

Therapeutic vectors carry drugs, genes and imaging agents into living cells and tissues.<sup>155–157</sup> The drugs vectors should also be stable in the circulatory system, yet become labile under appropriate conditions when the targeted organ is reached. The drug vectors carry the drug by encapsulation or more or less strong binding (covalent, coordination or supramolecular bond). The potential vectors include micelles, liposomes, steroids, folate, peptides, hyaluronic acid, fatty acids, antigens, polymers, dendrimers, nanotubes, and nanoparticles.<sup>9,10</sup> AuNPs have recently been considered as excellent drug-delivery systems due to their biocompatibility, optical properties and excellent abilities to bind (bioconjugation) biological ligands, DNA and small interfering RNA (siRNA) (noncovalent interaction) and drugs through AuNP surface bonding.<sup>158,159</sup> Specific applications can be classified in targeted drug delivery and mediated gene delivery. Targeted drug delivery has been achieved by endocytosis through a transmembrane receptor. For this purpose, AuNPs are conjugated to a ligand that specifically recognizes the receptor.

The protein transferrin has been conjugated to AuNPs, because many tumors cells overexpress transferrin receptors, and uptake of AuNP-transferrin by tumor cells has been characterized by AFM and confocal scanning laser microscopy.<sup>160</sup> PEG chains were anchored by thiotic acid and folic acid on opposite ends and conjugated to 10-nm AuNPs that proved to be stable in the pH 2–12 range and NaCl concentrations up to 0.5 M and could be taken up by folate-receptor-positive tumor cells. Cellular uptake was demonstrated by TEM of KB cells that actively express folate receptors on their membrane.<sup>161</sup> In a rare example of *in vivo* study, 26-nm AuNPs conjugated with the tumor-necrosis factor (TNF) were injected into tumor-bearing mice. They preferentially accumulated in the tumor and diminished the tumor mass

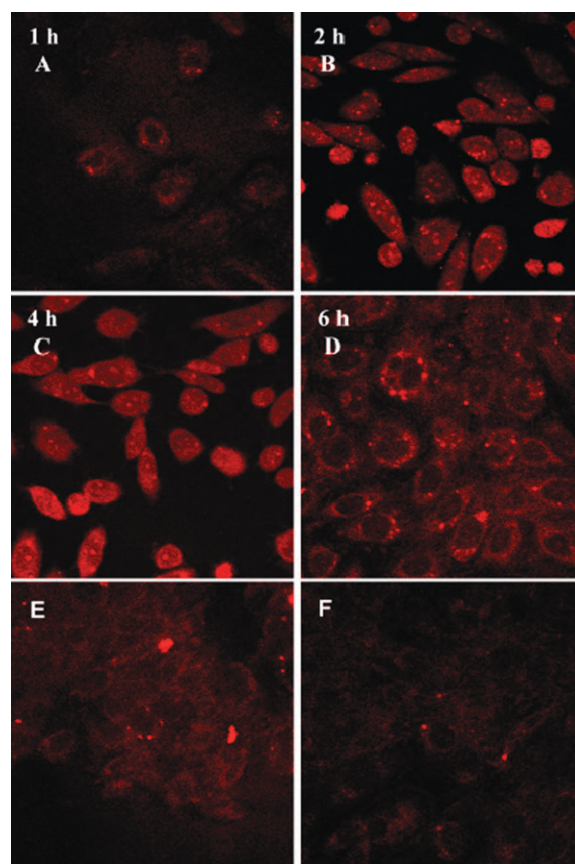


**Fig. 20** Cellular uptake and distribution of liposome entrapped gold nanoparticles in CHO cells. Images were taken after 1, 2, 4 and 6 h (A to D) incubation with liposome entrapped gold nanoparticles. Images E and F were taken after 1 and 2 h incubation when plain gold nanoparticles were used. Reprinted with permission of Elsevier (ref. 165, Devi's group).

more effectively than free TNF.<sup>162</sup> Enhanced efficacy of such AuNPs with a thiolated paclitaxel was also shown.<sup>163</sup>

A TEM study of 16-nm AuNPs conjugated with human fibroblast cells shows control of the uptake mechanism either *via* delivery of AuNPs by liposomes or by surface modification of the AuNPs with cell-penetrating peptides.<sup>164</sup> Liposome-entrapped AuNPs showed enhanced uptake by Chinese Hamster Ovary cells compared to liposome-free AuNPs (Fig. 20).<sup>165</sup> AuNPs were conjugated with transferrin molecules for imaging and therapy of breast cancer cells (Hs578T, ATCC). The transferrin/transferrin-receptor mediated cellular uptake of the AuNPs was six times of that in the absence of this interaction. The cellular uptake was only one fourth of that by the cancerous cells.<sup>166</sup> Tumor necrosis factor- $\alpha$  is a potent cytokine with anticancer efficacy, but it is systemically toxic, thereby needing selective delivery. Thus, the Paciotti group reported that PEG-33-nm AuNPs with incorporated TNF- $\alpha$  payload (several hundred TNF- $\alpha$  per AuNP) maximize tumor damage and minimize exposure to TNF- $\alpha$ .<sup>167,168</sup> Gene delivery is very promising, but common viral vectors raise cytotoxicity and immune response problems. Thus AuNP-based DNA-delivery vectors have been developed by Rotello's group first using cationic ligands, then with amphiphilic ligands that were more efficient on transfection.<sup>169,170</sup>

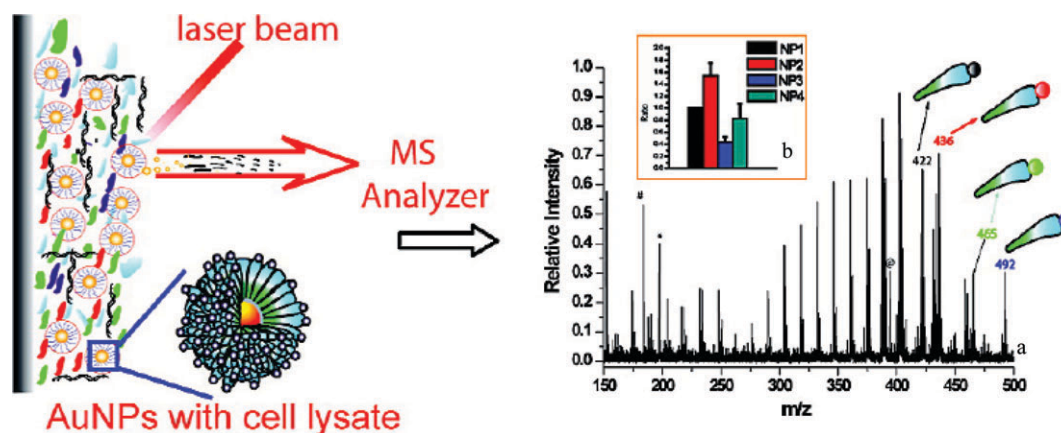


**Fig. 21** Schematic illustration of the analysis of the AuNPs in cell lysates by LDI-MS; (a) Multiplexed LDI mass spectrum of COS-1 cell lysate with the four cationic AuNPs 1–4.  $m/z$  422,  $m/z$  436,  $m/z$  492, and  $m/z$  465 correspond to AuNP 1, AuNP 2, AuNP 3, and AuNP 4, respectively. The symbol key is the same as in Fig. 3. (b) Relative amounts of AuNPs 1–4 obtained from LDI-MS. The AuNP amounts are normalized to that of AuNP 1. Reprinted with permission of Elsevier (ref. 174, Rotello's group).

Klibanov's group also reported the transfection efficiency of AuNP-PEI conjugates into kidney (Cos-7) cells.<sup>171</sup> Mirkin *et al.* showed the use of AuNPs conjugated to negatively-charged oligodeoxynucleotide for gene therapy,<sup>156</sup> and Rotello's group showed that intracellular concentrations of glutathione can trigger the restoration of DNA from cationic AuNP-NDA conjugate with potential applications in the creation of transfection vectors and gene-regulation systems.<sup>172</sup> Rotello *et al.* also reported photolabile AuNPs that provide light-regulated control over DNA-AuNP interactions, which is evidenced by a high level of DNA-transcription recovery *in vitro* and significant nuclear localization of DNA in cells.<sup>173</sup> The techniques that are available to characterize cell uptake by AuNPs carriers and intracellular probes are essentially luminescent imaging (including barcoding),

AFM and TEM. Multiplexed screening of cellular uptake has been demonstrated with laser-ionization mass spectrometry<sup>174</sup> (Fig. 21) and time-of-flight secondary ion mass spectrometry (TOF-SIMS).<sup>175</sup>

Adding polyelectrolyte-coated AuNRs to three-dimensional constructs composed of collagen and cardiac fibroblasts reduced contraction and altered the expression of mRNA encoding  $\gamma$ -actin,  $\alpha$ -smooth muscle actin and collagen type 1. These data show that AuNRs can modulate cell-mediated matrix remodeling and suggest that the targeted delivery of AuNRs can be applied for antifibrotic therapies.<sup>176</sup> Polyelectrolyte-AuNP-sensors are also based on refractive-index change.<sup>177</sup> "Gellan gum", widely used in food as a thickening and gelling agent, has been used in the reductive synthesis and stabilization of AuNPs that were applied to load anthracyclin

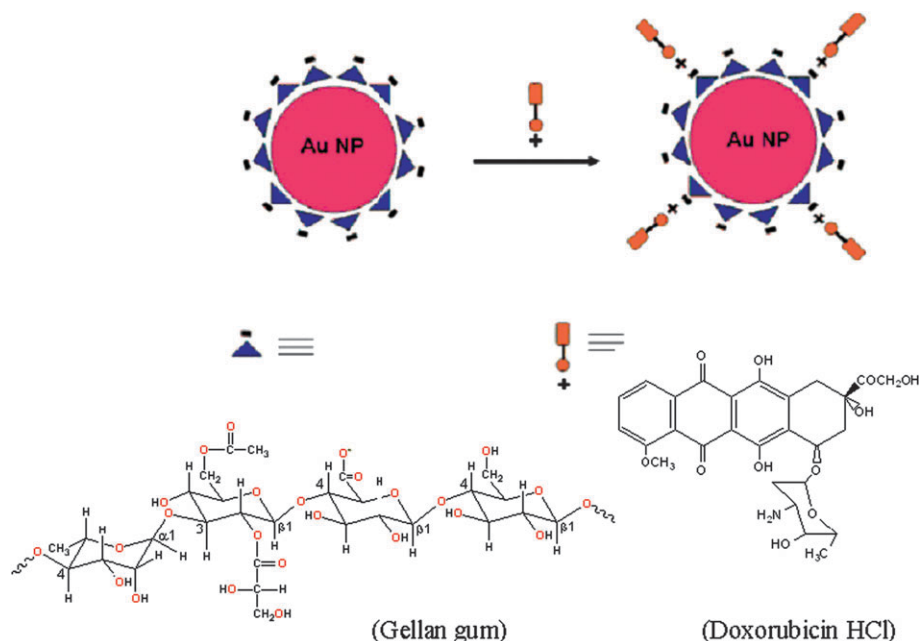


**Fig. 22** Schematic diagram showing anionic gellan gum gold nanoparticles and subsequent loading of cationic doxorubicin HCl on gellan gum capped gold nanoparticles. Reprinted with permission of Wiley InterScience (ref. 178, Prasad's group).

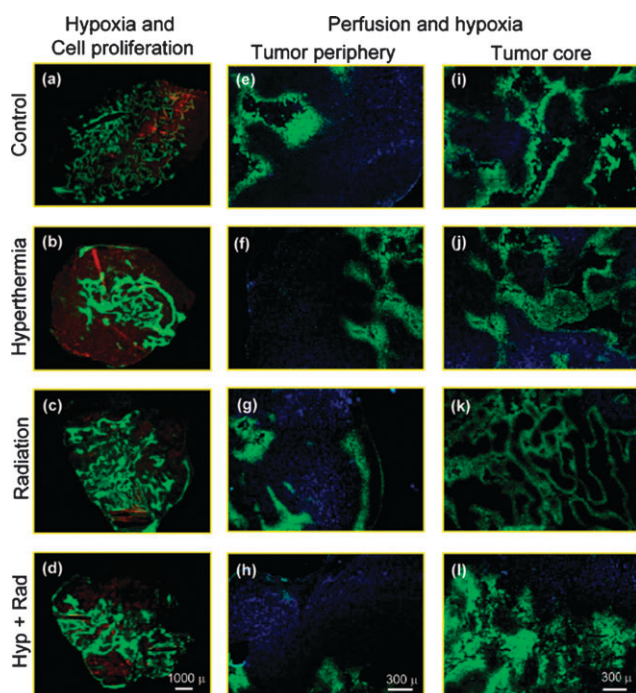


**Fig. 23** Immunofluorescence staining of control, hyperthermia, radiation, and thermoradiotherapy treated tumors showing hypoxia, cell proliferation (a–d), and hypoxia, perfusion in tumor periphery (e–h), and tumor core (i–l), respectively. Red, blue, and green fluorescence represents cell proliferation, perfusion, and hypoxic regions in tumors. Patchy hypoxic region seen in (l) is attributed to the vascular disruption effect induced by gold nanoshell-mediated thermoradiotherapy. Scale bars are represented in the bottom image of each column. Reprinted with permission of the American Chemical Society (ref. 182, Krishnan's group).

ring antibiotic doxorubicin hydrochloride. Such drug loading showed enhanced cytotoxic effects on human glioma cell lines LN-18 and LN-229 (Fig. 22).<sup>178</sup>

The Paciotti group has reported cryosurgery. The cytokine adjuvant TNF- $\alpha$  can be used to achieve complete cancer destruction at the periphery of an iceball (0 to  $-40^{\circ}\text{C}$ ). Although both surgery alone or TNF treatment alone caused only a minimal damage to the tumor tissues, the combination of TNF and cryosurgery produced a significant damage to the

tumor tissues.<sup>179,180</sup> The surfactant dodecylcysteine hydrochloride was reported to improve the antitumor activity of AuNPs in a cell line of the Ehrlich ascites carcinoma.<sup>181</sup> Hyperthermia of cancer cells using AuNPs appears essential to fight against intratumoral hypoxia that is a key mediator of the resistance of tumor cells to radiation therapy. Thus, an integrated antihypoxic and localized vascular disrupting therapeutic strategy was developed using tumor-vasculature-focused effects mediated by perivascularly sequestered AuNPs (Fig. 23).<sup>182</sup> Carbonic anhydrase inhibitors coated AuNPs were shown to selectively inhibit the tumor-associated isoform IX over the cytosolic isozymes I and II (Fig. 24).<sup>183</sup>

## 7. Cytotoxicity

The long history of (almost legendary) gold colloid use for therapeutic purposes suggests that AuNPs should be biocompatible. The considerable potential use of AuNPs in nanomedicine, especially for imaging, diagnostic and therapy requires, however, their toxicity to be thoroughly examined with maximum care and accuracy. The cytotoxicity of AuNPs, *i.e.* their cellular toxicity, has indeed been examined by several research groups and reviewed.<sup>184,185</sup> Since everything is toxic at high dose, the important question is whether AuNPs are toxic at the concentration at which they will be used, believed to be in the range of 1–100 AuNPs *per cell*.

### 7.1 Cytotoxicity *in vitro*

Some AuNPs can transfect cells. Rotello has shown that cationically functionalized alkylthiolate-AuNPs containing trimethylammonium ligand termini mediate DNA translocation across cell membranes in mammalian cells at a high level. Toxicity of these AuNPs was observed at concentrations only 2-fold higher than that found for maximal transfection activity. In fact, it is essential to distinguish between the toxicity of the AuNP core and that due to the ligands of the AuNP. In this case, it was shown that, whereas these cationic AuNPs are moderately toxic, the same alkylthiolate-AuNPs containing carboxylate termini are quite non-toxic. Accordingly, concentration-dependent lysis mediated by electrostatic binding was observed in dye release studies using lipid vesicles, suggesting the operating mechanism for the

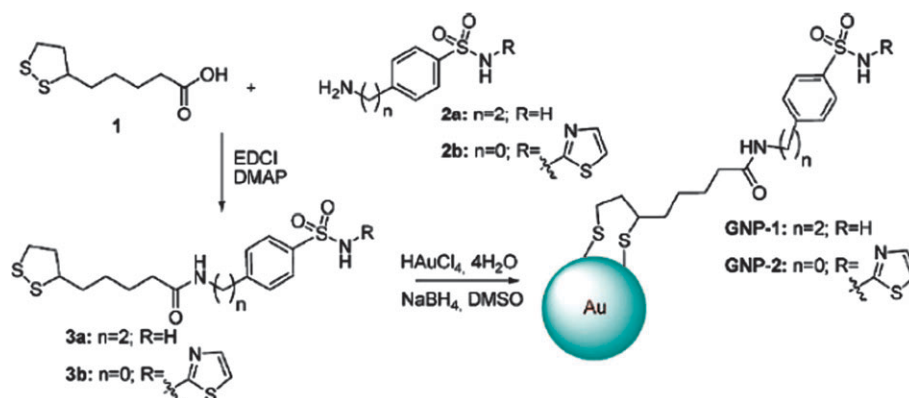


**Fig. 24** Synthesis of AuNPs coated with sulfonamide CAI, of type GNP-1 and GNP-2. Reprinted with permission of the American Chemical Society (ref. 183, Supuran's group).

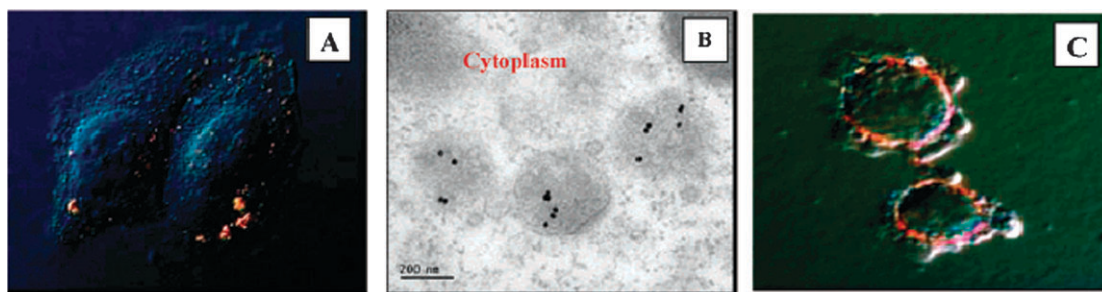


**Fig. 25** M1 nanoparticles incubated with HeLa cells. After 1 h, nanoparticles were observed by video-enhanced color differential interference contrast microscopy (A) and transmission electron microscopy (B) clustered in compartments inside the cytoplasm. After 2 h, nanoparticles were found accumulated around the nuclear membrane (C). Reprinted with permission of the American Chemical Society (ref. 188, Feldheim's group).

observed toxicity of these cationic AuNPs.<sup>186</sup> In another evidence of the key role of AuNP ligands, large AuNPs conjugated with biotin, cysteine, citrate, and glucose did not appear to be toxic in human leukemia (K562) cells at concentrations up to 250 mM in contrast to HAuCl<sub>4</sub> solutions were found to be 90% toxic.<sup>187</sup>

AuNP cytotoxicity may also eventually more or less depend on the cell lines, although this point is somewhat controversial, because differences observed might perhaps be due to variation of ligands (Fig. 25).<sup>188</sup> No physiological complication were found either in mice with AuNSs in another study.<sup>29</sup> Dose-dependent cytotoxicity was found with Au–Cu–NSs with 100% viability at low dose in mice, but 67% viability at high dose.<sup>189</sup> With AuNRs, strong cytotoxicity was associated with a low concentration of CTAB-stabilized AuNRs, and free CTAB was proposed to cause the toxicity.<sup>190,191</sup> Phosphatidylcholine was reported to reduce the cytotoxicity of CTAB-coated AuNRs.<sup>192</sup> It was pointed out that non-cytotoxic AuNPs can eventually cause cell damage, and abnormal filaments formation was produced by such 13-nm citrate-AuNPs.<sup>193</sup> AuNRs coated with layer-by-layer polyelectrolytes such as the common poly(diallyldimethylammonium chloride)-poly(4-styrenylsulfonic acid) showed low toxicity and were considered as well suited for therapeutic applications.<sup>194</sup> The cytotoxicity of AuNPs conjugated with PEGylated biotin-PEG-poly( $\epsilon$ -caprolactone) copolymers towards Caco-2 cells in culture was shown to be negligible.<sup>195</sup>

## 7.2 Cytotoxicity *in vivo*

The full potential of innovations in terms of AuNP medical use can only be achieved with the concomitant realization of *in vivo* profiles for pharmacological intervention.<sup>196</sup> Different routes of administration can result in various effects on the biodistribution of drug carriers.<sup>197</sup> Subcutaneous, intramuscular or topical administration of colloidal drug carriers generally results in retention of the drug carrier for longer time than free drug, and these drug carriers are mainly retained by local lymph nodes.<sup>198,199</sup> *In vivo* distribution subsequent to administration largely depends on NP size, surface charge and surface hydrophobicity.<sup>200,201</sup> The influence of these factors on the uptake of NPs by the mononuclear phagocyte system has been described.<sup>201</sup> The presence of biocompatible amphiphilic chains on NP surface decreases phagocytosis of the NPs by the

non-parenchymal cells of the liver, allowing longer circulation time in blood.<sup>202</sup> Permeation of small AuNPs through skin and intestine was found to be size dependent.<sup>203</sup> The biological distribution of various sizes (15, 50, 100 and 200 nm) of AuNPs on intravenous administration in mice was investigated and revealed that AuNPs of all sizes were mainly accumulated in liver, lung and spleen, whereas accumulation in various tissues depended on AuNP size. High amounts of 15-nm AuNPs were found in all tissues including blood, liver, lung, spleen, kidney, and stomach and were able to pass the blood-brain barrier, as 50-nm AuNPs also did. On the other hand, only minute amount of 200-nm AuNPs were found in blood, brain, stomach and pancreas.<sup>204</sup> Accordingly, in another study, rats intravenously injected with AuNPs of 10-, 50-, 100- and 250-nm diameters were shown to contain the 10-nm AuNPs in the various organs, whereas larger AuNPs were only detected in blood, liver and spleen.<sup>205</sup> The Paciotti group reported that the tumor-necrosis factor (TNF)-conjugated AuNPs show similar antitumor effects to TNF alone, but with less systemic toxicity in mice.<sup>206</sup> Studies of biodistribution of 1.4-nm and 1.8-nm AuNPs that were administrated by intravenous injection or intratracheal instillation in rats indicated that the 1.4-nm AuNPs can be translocated through the air/blood barrier of the respiratory tract in significant amounts, whereas the 1.8-nm AuNPs are almost completely trapped in the lungs. Additionally, there is evidence that the AuNPs are modified during the translocation process.<sup>207</sup> In a study of pharmacokinetics and biodistribution in nude mice of PEG-coated AuNPs, AuNPs coated with thioctic acid-anchored PEG exhibited higher colloidal stability in phosphate-buffered saline in the presence of dithiothreitol than did AuNPs coated with monothiol-anchored PEG. AuNPs coated with 5000-Da PEG were more stable than those coated with 2000-Da PEG. Of the 20-nm, 40-nm, and 80-nm AuNPs coated with thioctic acid-terminated 5000-Da PEG, the 20-nm AuNPs exhibited the lowest uptake by retinoendothelial cells and the lowest clearance by the body, and showed significantly higher tumor uptake and extravasation from the tumor blood vessels than did the 40- and 80-nm AuNPs.<sup>208</sup>

Although all these studies show the AuNP size distribution, it would also be of interest in the future to obtain information on the influence of other AuNP characteristics such as morphology, crystallinity, surface defects, charge and reactivity.

### 7.3 Conclusion on toxicity studies

In conclusion to the toxicity survey, it appears that AuNPs usually show rather little toxicity, if any, because many cytotoxicity studies report negative cytotoxicity finding results. The cationic ligands of AuNPs, however, clearly cause moderate toxicity, and some toxicity may also be specific to other types of ligands. A systematic toxicity study must be carried out for each specific case under precise conditions, before imaging, diagnosis and therapeutic applications of AuNPs can be carried out in human. Also, *in vivo* conditions are different from *in vitro* results, and in particular more *in vivo* studies are called for. Thus, no general conclusion can be drawn at present. It has been suggested, however, that it could be applicable to use AuNPs as reference nanoparticles for low toxicity in the set-up of a nanoparticle toxicity scale, given the higher toxicity of carbon nanotubes and quantum dots compared to non-cationic AuNPs. Finally, AuNPs are redox active and therefore reduce the production of reactive oxygen- and nitrite species.<sup>209</sup> The non-cytotoxicity, non-immunogenicity and biocompatibility of many AuNPs make us relatively optimistic concerning their future essential applications in nanomedicine.

## 8. Conclusion and outlook

Medically useful AuNPs can be prepared and stabilized (conjugated) with a large variety of stabilizers (citrate, various ligands, polymers, dendrimers, surfactants) including biomolecules such as oligonucleotides and DNA. The best stabilizers are thiolates (for instance oligonucleotides modified with a thiolate group). New practical stabilizers such as “gellan gum” exemplify this variety.<sup>178</sup> Thiolated PEGs are especially useful because they masks AuNPs from the intravascular immune system and help targeting cancer cells due to the EPR effect.

The surface plasmon absorption of AuNPs provides outstanding optical properties that can be used with a variety of techniques for labeling, imaging, sensing leading to both diagnostics and therapies. This SPB is extremely dependent on the surface, AuNP shape, inter-AuNP distance, medium (refractive index) and ligands, which makes the basis for molecular recognition, imaging and sensing sensitivity. The most famous example of sensor is Mirkin's “*Northwestern spot test*”, a visual record of the inter-AuNP distance-dependent color change and temperature-dependent disaggregation (melting) that can detect mismatched DNA.<sup>54</sup>

Modern spectroscopic techniques, such as SERS that provides a huge enhancement of the Raman signal, by a factor of *ca.*  $10^{14}$ – $10^{15}$ , allowing detection at the single molecule level,<sup>210</sup> considerably facilitates the diagnostic of cancer and other diseases (SERS combines *elastically* scattered visible light from the AuNP themselves that can be imaged using a dark-field optical microscope with *inelastic* SERS effect due to adsorbed molecules providing a Raman spectrum leading to the identification of biomolecules). For instance, antibody-modified AuNPs displayed a million-fold higher sensitivity than conventional ELISA-based assay in the detection of prostate specific antigen (PSA).<sup>211</sup>

A number of other useful optical and electrochemical techniques including fluorescence, Ag staining and electrocatalytic biosensors have been discussed here. These biosensing techniques allow clinical diagnosis of cancer, Alzheimer, HIV, hepatitis B, tuberculosis, diabetes and arthritis.

In the cancer therapy section, it was shown how photothermal AuNP NIR irradiation of cancer cells combines both diagnosis (imaging) and selective therapy, a technique also applicable to other diseases. In addition, the discovery that the SPB can be shifted from the visible region for spherical AuNPs to the NIR region for AuNRs and AuNSs led the groups of Halas,<sup>28</sup> Murphy<sup>26</sup> and El-Sayed<sup>140</sup> to introduce a breakthrough with the extension of the efficient use of the SPB for cancer therapy, a non-invasive method with efficient tumor ablation in the NIR region where blood and tissues are less absorbing (“biological window”: 650–900 nm).<sup>29</sup>

Techniques that do not use the SPB, however, such as RF heating of AuNPs and AuP-targeting with singlet oxygen therapy are also known. Indeed, the use of AuNPs as vectors is very general, because it can be directly applied in a non-invasive way for various therapies including angiogenesis, anti-bacterial treatments, *etc.*

Drug delivery (both drugs and DNA) appears as one of the most promising future applications of AuNPs, as exemplified by a number of recent reports that were reviewed here. For instance AuNP-based DNA-delivery vectors have been developed by Rotello who showed that intracellular concentrations of glutathione can trigger the restoration of DNA with potential applications in the creation of transfection vectors.<sup>172</sup> Mirkin showed the use of AuNPs conjugated to oligodeoxynucleotide for gene therapy.<sup>156</sup> The Paciotti group reported cryosurgery, indicating that the combination of TNF- $\alpha$  and cryosurgery produced a significant damage to the tumor tissues.<sup>179,180</sup>

Finally, a very important problem in potential therapy for human is that of toxicity that must be carefully and precisely studied. Many groups have reported the non-toxicity of AuNPs. One must distinguish between the toxicity of the AuNP core and that of ligands. Cationic ligands including CTAB appear moderately toxic, and some other ligands also may be toxic. Many biocompatible ligands including thiolated PEGs are non-toxic, however. AuNPs appear much less toxic than other types of nanoparticles, and one should be reasonably optimistic concerning potential applications. In conclusion, AuNPs are biocompatible, easily bio-conjugable and very promising for imaging, diagnostics and therapy biomedical applications for cancer and a number of other diseases for human.<sup>7</sup>

### List of abbreviations

AFM	Atomic force microscopy
ATP	Adenosine triphosphate
AuNPs	Gold nanoparticles
AuNRs	Gold nanorods
AuNSs	Gold nanoshells
CCD	Charge-coupled device
CCR5	Chemokine CC motif receptor 5
CD	Compact disc

CEA	Carcinoembryonic antigen
CTAB	Cetyl trimethylammonium bromide
Cy	Cyanine
DIC	Differential interference contrast
DLSS	Differential light-scattering spectroscopy
DNA	Deoxyribonucleic acid
ECL	Electrogenerated chemiluminescence
EDC	1-Ethyl-3(3-dimethylaminopropyl)-carbodiimide-HCl
EGFR	Epithelial growth factor receptor
EIS	Electrochemical impedance spectroscopy
ELISA	Enzyme-linked immunosorbent assay
FCS	Fluorescence correlation spectroscopy
FRET	Fluorescence resonance energy transfer
GO	Glucose oxidase
HBV	Hepatitis B virus
HEK	Human embryonic kidney
HER2	Human epidermal growth factor receptor 2
HIV	Human immunodeficiency virus
HOC	Human ovarian cancer
HRS	Hyper-Raleigh scattering
HSC	Hematopoietic stem cells
IC <sub>50</sub>	Half maximal inhibitory concentration
IgG	Immunoglobulin G
IR	Infrared
MRI	Magnetic resonance imaging
mRNA	Messenger ribonucleic acid
Nd-YAG	Neodymium-doped yttrium aluminium garnet
NIR	Near infrared
PCT	Photothermal coherence tomography
PCR	Polymerase chain reaction
PEG	Polyethylene glycol
PEI	Polyethylene imine
PLC	Phospholipase C
PSA	Prostate specific antigen
RCM	Reflection contrast microscopy
RF	Radiofrequency
RNA	Ribonucleic acid
ScFv	Single-chain variable-fragment
SDC	Shielded dynamic complex-gate
SELEX	Systematic evolution of ligands by exponential enrichment
SERS	Surface-enhanced Raman scattering
siRNA	Small interfering ribonucleic acid
SNPs	Single nucleotide polymorphisms
SPB	Surface plasmon band
SPR	Surface plasmon resonance
TEM	Transmission electron microscopy
TNF	Tumor-necrosis factor
TOF-SIMS	Time-of-flight secondary mass spectrometry
UV	Ultraviolet

## Acknowledgements

We are grateful to the Université Bordeaux I, the Centre National de la Recherche Scientifique (CNRS), the Institut Universitaire de France (IUF, DA) and the Agence Nationale de la Recherche (ANR) for financial support.

## References

- W. P. Faulk and G. M. Taylor, *Immunochemistry*, 1971, **8**, 1081–1083.
- G. M. Whitesides, *Nat. Biotechnol.*, 2003, **21**, 1161–1165.
- E. Katz and I. Willner, *Angew. Chem., Int. Ed.*, 2004, **43**, 6042–6108.
- N. L. Rosi and C. A. Mirkin, *Chem. Rev.*, 2005, **105**, 1547.
- D. Astruc, *C. R. Acad. Sci.*, 1996, **322**(Série II b), 757–766.
- U. Dreshler, B. Erdogan and V. M. Rotello, *Chem.–Eur. J.*, 2004, **10**, 5570–5579.
- R. Langer and D. A. Tirrell, *Nature*, 2004, **428**(6982), 487–492.
- M. Ferrari, *Nat. Rev. Cancer*, 2005, **5**, 161–171.
- T. Ganesh, *Bioorg. Med. Chem.*, 2007, **15**(1), 3597–3623.
- P. K. Jain, X. Huang, I. H. El-Sayed and M. A. El-Sayed, *Plasmonics*, 2007, **2**, 107–118.
- M. Faraday, *Philos. Trans. R. Soc. London*, 1857, **147**, 145–181.
- G. Mie, *Ann. Phys.*, 1908, **25**, 377–445.
- M.-C. Daniel and D. Astruc, *Chem. Rev.*, 2004, **104**, 293–346 and refs. cited therein.
- M. Tréguer-Delapierre, J. Majimel, S. Mornet and S. Ravaine, *Gold Bull.*, 2008, **41**(2), 195–207.
- J. Turkevitch, P. C. Stevenson and J. Hillier, *Discuss. Faraday Soc.*, 1951, **11**, 55–75.
- J. Kimling, M. Maier, B. Okenve, V. Kotaidis, H. Ballot and A. Plech, *J. Phys. Chem. B*, 2006, **110**, 5700–5707.
- M. Giersig and P. Mulvaney, *Langmuir*, 1993, **9**, 3408–3413 and refs. cited therein.
- M. Brust, M. Walker, D. Bethell, D. J. Schiffrin and R. J. Whyman, *J. Chem. Soc., Chem. Commun.*, 1994, 801–802.
- A. C. Templeton, W. P. Wuelfing and R. W. Murray, *Acc. Chem. Res.*, 2001, **33**, 27–36.
- R. A. Sperling, P. Rivera Gil, F. Zhang, M. Zanella and W. J. Parak, *Chem. Soc. Rev.*, 2008, **37**, 1896–1908 and refs. cited therein.
- H. C. Kolb, M. G. Finn and K. B. Sharpless, *Angew. Chem., Int. Ed.*, 2001, **40**, 2004–2021.
- E. Boisselier, L. Salmon, J. Ruiz and D. Astruc, *Chem. Commun.*, 2008, 5788–5790.
- R. W. J. Scott, O. M. Wilson and R. M. Crooks, *J. Phys. Chem. B*, 2005, **109**, 692–704 and refs. cited therein.
- E. Boisselier, A. K. Diallo, L. Salmon, J. Ruiz and D. Astruc, *Chem. Commun.*, 2008, 4819–4821.
- H. Wu, H. Zhu, J. Zhang, S. Yang, C. Liu and Y. C. Cao, *Angew. Chem., Int. Ed.*, 2008, **47**, 3730–3734.
- C. J. Murphy, A. M. Gole, S. E. Hunyadi, J. W. Stone, P. N. Sisco, A. Alkilany, B. E. Kinard and P. Hankins, *Chem. Commun.*, 2008, 544–557 and refs. cited therein.
- X. H. Huang, P. K. Jain, I. H. El-Sayed and M. El-Sayed, *Laser Med. Sci.*, 2008, **23**, 217–228 and refs. cited therein.
- S. L. Lal, S. E. Clare and N. J. Halas, *Acc. Chem. Res.*, 2008, **41**(12), 1842–1851 and refs. cited therein.
- T. Niidome, M. Yagamata, Y. Okamoto, Y. Akiyama, H. Takahashi, T. Kawano, Y. Katayama and Y. Niidome, *J. Controlled Release*, 2006, **114**(3), 343–347.
- M. Z. Liu and P. Guyot-Sionnest, *J. Phys. Chem. B*, 2005, **109**, 22192–22200.
- G. F. Paciotti, D. G. I. Kinston and L. Tamarkin, *Drug Dev. Res.*, 2006, **5**, 2255–2262 and refs. cited therein.
- L. M. Liz Marzan, *Langmuir*, 2006, **22**, 32–41 and ref. cited therein.
- M. C. Skala, M. J. Crow, A. Wax and J. A. Izatt, *Nano Lett.*, 2008, **8**(10), 3461–3467.
- D. Yelin, D. Oron, S. Thiberge, E. Moses and Y. Silberberg, *Opt. Express*, 2003, **11**(12), 1385–1391.
- P.-J. Debouttière, S. Roux, F. Vocanson, C. Billotey, O. Bæuf, A. Favre-Régouillon, Y. Lin, S. Pellet-rostaing, R. Lamartine, P. Perriat and O. Tillement, *Adv. Funct. Mater.*, 2006, **16**, 2330–2339.
- Y. T. Lim, M. Y. Cho, J. K. Kim, S. Hwangbo and B. H. Chung, *ChemBioChem*, 2007, **8**, 2204–2209.
- T. A. Larson, J. Bankson, J. Aaron and K. Sokolov, *Nanotechnology*, 2007, **18**, 325101.
- X. Ji, R. Shao, A. M. Elliott, R. J. Stafford, E. Esparza-Coss, J. A. Bankson, G. Liang, Z.-P. Luo, K. Park, J. T. Markert and C. Li, *J. Phys. Chem. C*, 2007, **111**, 6245–6251.

- 39 J.-s. Choi, H. J. Choi, D. C. Jung, J.-H. Lee and J. Cheon, *Chem. Commun.*, 2008, 2197–2199.
- 40 J. Aaron, N. Nitin, K. Travis, S. Kumar, T. Collier, S. Y. Park, M. Jose-Yacamán, L. Coghlan, M. Follen, R. Richards-Kortum and K. Sokolov, *J. Biomed. Opt.*, 2007, **12**(3), 034007.
- 41 X. H. Huang, P. K. Jain, I. H. El-Sayed and M. A. El-Sayed, *Lasers Med. Sci.*, 2008, **23**, 217–228.
- 42 X. H. Huang, I. H. El-Sayed, W. Qian and M. A. El-Sayed, *Nano Lett.*, 2007, **7**(6), 1591–1597.
- 43 S. W. Bishnoi, C. J. Rozell, C. S. Levin, M. K. Gheith, B. R. Johnson, D. H. Johnson and N. J. Halas, *Nano Lett.*, 2006, **6**, 1687–1692.
- 44 R. Wilson, A. R. Cossins and D. G. Spiller, *Angew. Chem., Int. Ed.*, 2006, **45**, 6104.
- 45 R. Wilson, *Chem. Soc. Rev.*, 2008, **37**, 2028–2045.
- 46 W. E. Doering, M. E. Piotti, M. J. Natan and R. G. Freeman, *Adv. Mater.*, 2007, **19**, 3100–3108.
- 47 Q. Hu, L.-L. Tay, M. Noestheden and J. P. Pezacki, *J. Am. Chem. Soc.*, 2007, **129**, 14–15.
- 48 J. Kneipp, H. Kneipp, B. Wittig and K. Kneipp, *Nano Lett.*, 2007, **7**, 2819–2823.
- 49 X. Qian, X.-H. Peng, D. O. Ansari, Q. Yin-Goen, G. Z. Chen, Dong M. Shin, L. Yang, A. N. Young, M. D. Wang and S. Nie, *Nat. Biotechnol.*, 2008, **26**, 83–90.
- 50 S. Lee, S. Kim, J. Choo, S. Y. Shin, Y. H. Lee, H. Y. Choi, S. Ha, K. Kang and C. H. Oh, *Anal. Chem.*, 2007, **79**, 916–922.
- 51 J. H. W. Leuvening, P. J. H. M. Thal, M. van der Waart and A. H. W. M. Schuur, *Fresenius Z. Anal. Chem.*, 1980, **301**, 132–132.
- 52 C. X. Zhang, Y. Zhang, X. Wang, Z. M. Tang and Z. H. Lu, *Anal. Biochem.*, 2003, **320**, 136–140.
- 53 C. A. Mirkin, R. L. Letsinger, R. C. Mucic and J. J. Storhoff, *Nature*, 1996, **382**, 607–609.
- 54 R. Elghanian, J. J. Storhoff, R. C. Mucic, R. L. Letsinger and C. A. Mirkin, *Science*, 1997, **75**, 1078–1081.
- 55 D. Murphy and G. Redmond, *Anal. Bioanal. Chem.*, 2005, **381**, 1122–1129.
- 56 J. H. Li, X. Chu, Y. L. Liu, J. H. Jiang, Z. He, Z. Zhang, G. J. Chen and R. Q. Yu, *Nucleic Acids Res.*, 2005, **33**, E168.
- 57 B. M. Reinhard, M. Siu, H. Agarwal, A. P. Alivisatos and J. Liphardt, *Nano Lett.*, 2005, **5**, 2246–2252.
- 58 J. Stehr, C. Hrelescu, B. D. Sperling, G. Raschke, M. Wunderlich, A. Nichtl, D. Heindl, K. Krzinger, W. J. Parak, T. A. Klar and J. Felmann, *Nano Lett.*, 2008, **8**, 619–622.
- 59 J. N. Nam, S. I. Steva and C. A. Mirkin, *J. Am. Chem. Soc.*, 2004, **126**, 5932–5933.
- 60 X. Y. Xu, M. S. Han and C. A. Mirkin, *Angew. Chem., Int. Ed.*, 2007, **46**, 3468–3470.
- 61 P. Batista, E. Pereira, P. Eaton, G. Doria, A. Miranda, I. Gomes, P. Quaresma and R. Franco, *Anal. Bioanal. Chem.*, 2008, **391**, 943–950.
- 62 J. W. Liu and Y. Lu, *Org. Biomol. Chem.*, 2006, **4**, 3435–3441.
- 63 L. R. Hirsch, J. B. Jackson, A. Lee, N. J. Halas and J. West, *Anal. Chem.*, 2003, **75**, 2377–2381.
- 64 L. R. Hirsch, A. M. Gobin, A. R. Lowery, F. Tam, R. A. Drezek, N. J. Halas and J. L. West, *Ann. Biomed. Eng.*, 2006, **34**, 15–22 and refs. cited therein.
- 65 A. Gole and C. J. Murphy, *Langmuir*, 2005, **21**(23), 10756–10762.
- 66 E. Dujardin, L.-B. Hsin, C. R. C. Wang and S. Mann, *Chem. Commun.*, 2001, 1264–1265.
- 67 J. K. N. Mbindyo, B. D. Reiss, B. R. Martin, C. D. Keating, M. J. Natan and T. E. Mallouk, *Adv. Mater.*, 2001, **13**(4), 249–254.
- 68 C. Y. Chang, H. Wu, H. Chen, Y.-C. Ling and W. Tan, *Chem. Commun.*, 2005, **8**, 1092–1093.
- 69 X. Li, L. Jiang, Q. Zhan, J. Qian and S. He, *Colloids Surf., A*, 2009, **332**, 172–179.
- 70 G. J. Nusz, S. M. Marinakos, A. C. Curry, A. Dahlin, F. Hok, A. Wax and A. Chilkoti, *Anal. Chem.*, 2008, **80**, 984–989.
- 71 V. Pavlov, Y. Xiao, B. Shlyahovsky and I. Wilner, *J. Am. Chem. Soc.*, 2004, **126**, 11768–11769.
- 72 W. Eck, G. Craig, A. Sigdel, G. Ritter, L. J. Old, L. Tang, M. F. Brennan, P. J. Alle and M. D. Mason, *ACS Nano*, 2008, **2**, 2263–2272.
- 73 T. A. Taton, C. A. Mirkin and R. L. Letsinger, *Science*, 2000, **289**, 1157–1160.
- 74 S. A. Lange, G. Roth, S. Wittermann, T. Lacoste, A. Vetter, J. Grassle, S. Kopta, M. Kolbeck, B. Breiter, M. Wick, J. K. H. Horber, S. Dubel and A. Bernard, *Angew. Chem., Int. Ed.*, 2006, **45**, 270–273.
- 75 R. Martins, P. Batista, L. Silva, L. Raniero, G. Doria, R. Franc and E. Fortunato, *J. Non-Cryst. Solids*, 2008, **354**, 2580–2584.
- 76 R. Wilson, *Chem. Commun.*, 2003, 108–109.
- 77 H. He, C. Xie and J. Ren, *Anal. Chem.*, 2008, **80**, 5951–5957.
- 78 P. C. Ray, G. K. Darbha, A. Ray, J. Walker and W. Hardy, *Plasmonics*, 2007, **2**, 173–183.
- 79 T. Pons, I. L. Medintz, K. E. Sapsford, S. Higashiyama, A. F. Grimes, D. S. English and H. Mattoussi, *Nano Lett.*, 2007, **7**, 3157–3164.
- 80 C. C. You, O. R. Miranda, B. Gider, P. S. Ghosh, I. B. Kim, B. Erdogan, S. A. Krovi, U. H. F. Bunz and V. M. Rotello, *Nat. Nanotechnol.*, 2007, **2**, 318–323.
- 81 S. Lee, E.-J. Cha, K. Park, S.-Y. Lee, J. K. Hong, I.-C. Sun, S. Y. Kim, K. Choi, I. C. Kwon, K. Kim and C.-H. Ahn, *Angew. Chem., Int. Ed.*, 2008, **47**, 2804–2807.
- 82 D. Astruc, *Electron Transfer and Radical Processes in Transition Metal Chemistry*, VCH, New York, 1995, ch. 4 and 7.
- 83 M. Dequaire, C. Degrand and B. Limoges, *Anal. Chem.*, 2000, **72**, 5521–5528.
- 84 M. Pumer, S. Sanchez, I. Ichinose and J. Tang, *Sens. Actuators*, 2007, **123**, 1195–1205 and refs. therein.
- 85 S. Guo and E. Wang, *Anal. Chim. Acta*, 2007, **598**, 181–192 and refs. cited therein.
- 86 M. T. Castaneda, S. Alegret and A. Merkoçi, *Electroanalysis*, 2007, **19**, 743–753.
- 87 Y. Xiao, F. Patolsky, E. Katz, J. F. Hainfeld and I. Willner, *Science*, 2003, **299**, 1877–1881.
- 88 P. Scodeller, V. Flexer, R. Szamocki, E. J. Calvo, N. Tognalli, H. Troiani and A. Fainstein, *J. Am. Chem. Soc.*, 2008, **130**, 12690–12697.
- 89 Y. Wang, W. Wei, X. Liu and X. Zeng, *Mater. Sci. Eng., C*, 2009, **29**, 50–54.
- 90 D. Tang, R. Yuan, Y. Chai, Y. Fu, J. Dai, Y. Liu and X. Zhong, *Biosens. Biochem.*, 2005, **21**, 539–548.
- 91 J. Manso, N. M. L. Mena, P. Yáñez-Sedeño and J. M. Pingarrón, *Anal. Biochem.*, 2008, **375**, 345–353.
- 92 J. Lin, C. He, L. Zhang and S. Zhang, *Anal. Biochem.*, 2009, **384**, 130–135.
- 93 L. Authier, C. Grossiord, P. Grossier and B. Limoges, *Anal. Chem.*, 2001, **73**, 4450–4456.
- 94 J. Wang, A. Xu and R. Polsky, *J. Am. Chem. Soc.*, 2002, **124**, 4208–4209 and refs. cited therein.
- 95 K. Idegami, M. Chikae, K. Kerman, N. Nagatani, T. Yuki, T. Endo and E. Tamiya, *Electroanalysis*, 2008, **20**, 14–21.
- 96 K. Hu, D. Lan, X. Li and S. Zhang, *Anal. Chem.*, 2008, **80**, 9124–9130.
- 97 H. Wang, C. X. Zhang, Y. Li and H. L. Qi, *Anal. Chem.*, 2006, **78**, 505–511.
- 98 A. Becue, C. Champod and P. Margot, *Forensic Sci. Int.*, 2007, **168**, 169.
- 99 M. Yamada and H. Nishihara, *C. R. Chim.*, 2003, **6**(8–10), 919–934 and refs. cited therein.
- 100 A. Labande, J. Ruiz and D. Astruc, *J. Am. Chem. Soc.*, 2002, **124**, 1782–1789.
- 101 M.-C. Daniel, J. Ruiz and D. Astruc, *J. Am. Chem. Soc.*, 2003, **125**, 1150–1151.
- 102 M.-C. Daniel, J. Ruiz, S. Nlate, J.-C. Blais and D. Astruc, *J. Am. Chem. Soc.*, 2003, **125**, 2617–2628.
- 103 D. Astruc, C. Ornelas and J. Ruiz, *Acc. Chem. Res.*, 2008, **41**, 841–856.
- 104 C. Valerio, J.-L. Fillaut and J. Ruiz, *J. Am. Chem. Soc.*, 1997, **119**, 2588–2589.
- 105 R. Tanaka, T. Yuhi, N. Nagatani, T. Endo, K. Kerman, Y. Takamura and E. Tamiya, *Anal. Bioanal. Chem.*, 2006, **385**, 1414–1420.
- 106 N. S. Lai, C. C. Wang, H. L. Chiang and L. K. Chau, *Anal. Bioanal. Chem.*, 2007, **388**, 901–907.
- 107 B. Y. Hsieh, Y. F. Chang, M. Y. Ng, W. C. Liu, C. H. Lin, H. T. Wu and C. Chou, *Anal. Chem.*, 2007, **79**, 3487–3493.

- 108 Z. P. Wang, J. Q. Hu, Y. Jin, X. Jiao and J. H. Li, *Clin. Chem.*, 2006, **52**, 1958–1961.
- 109 L. R. Hirsch, J. B. Jackson, A. Lee, N. J. Halas and J. L. West, *Anal. Chem.*, 2003, **75**, 2377–2381.
- 110 C. P. Chan, Y. C. Cheung, R. Renneberg and M. Seydack, *Adv. Biochem. Eng. Biotechnol.*, Springer, Heidelberg, 2007.
- 111 C. Ou, R. Yuan, Y. Chai and X. He, *Anal. Chim. Acta*, 2007, **603**, 205–213.
- 112 J. Lin, W. Qu and S. Zhang, *Anal. Sci.*, 2007, **23**, 1059–1063.
- 113 C. Yu and J. Irudayaraj, *Anal. Chem.*, 2007, **79**, 572–579.
- 114 S.-H. Chen, V. C. H. Wu, Y.-C. Chuang and C.-S. Lin, *J. Microbiol. Methods*, 2008, **73**, 7–17.
- 115 K. Sokolov, M. Follen, J. Aaron, I. Pavlova, A. Malpica, R. Lotan and R. Richards-Kortum, *Cancer Res.*, 2003, **63**, 1999–2004.
- 116 V. Dixit, J. van der Bossche, D. M. Sherman, D. H. Thompson and R. P. Andres, *Bioconjugate Chem.*, 2006, **17**, 603–609.
- 117 I. H. El-Sayed, X. H. Huang and M. A. El-Sayed, *Nano Lett.*, 2005, **5**, 829–834.
- 118 X. H. Huang, P. K. Jain, I. H. El-Sayed and M. A. El-Sayed, *Future Nanomed.*, 2007, **2**, 681–693.
- 119 G. Doria, R. Franco and P. Batista, *IET Nanobiotechnol.*, 2007, **1**, 53–57.
- 120 L. G. Carascosa, M. Moreno, M. Alvarez and L. M. Lechuga, *Trends Anal. Chem.*, 2006, **25**, 196–206.
- 121 C. M. Medley, J. E. Smith, Z. Tang, Y. Wu, S. Bamrungsap and W. Tan, *Anal. Chem.*, 2008, **80**, 1067–1072.
- 122 P. Podsiadlo, V. A. Sinani, J. H. Bahng, N. W. S. Kam, J. Lee and N. A. Kotov, *Langmuir*, 2008, **24**, 568–574.
- 123 M. Eghtedari, A. V. Liopo, J. A. Copland, A. A. Oraevsky and M. Motamedi, *Nano Lett.*, 2009, **9**, 287–291.
- 124 A. J. Haes, W. P. Hall, L. Chang, W. L. Klein and R. P. Van Duyne, *Nano Lett.*, 2004, **4**, 1029–1034.
- 125 A. J. Haes, L. Chang, W. L. Klein and R. P. Van Duyne, *J. Am. Chem. Soc.*, 2005, **127**, 2264–2271.
- 126 D. G. Georgopoulos, L. Chang, J. M. Nam, C. S. Taxton, E. J. Mufson, W. L. Klein and C. A. Mirkin, *Proc. Natl. Acad. Sci. U. S. A.*, 2005, **102**, 2273–2276.
- 127 M.-C. Bowman, T. E. Ballard, C. J. Ackerson, D. L. Feldheim, D. M. Margolis and C. Melander, *J. Am. Chem. Soc.*, 2008, **130**, 6896–6897.
- 128 K. A. Mahmoud and J. H. T. Luong, *Anal. Chem.*, 2008, **80**, 7056–7062.
- 129 D. Xi, X. Luo, Q. Ning, Q. Lu, K. Yao and Z. Liu, *J. Nanjing Med. Univ.*, 2007, **21**(4), 207–212.
- 130 P. V. Baptista, M. Koziol-Montewka, J. Paluch-Oles, G. Doria and R. Franco, *Clin. Chem.*, 2006, **52**, 1433–1434.
- 131 L. R. Hirsch, R. J. Stafford, J. A. Bankson, S. R. Sershen, B. Rivera, R. E. Price, J. D. Hazle and N. J. Halas, *Proc. Natl. Acad. Sci. U. S. A.*, 2003, **100**, 13549–13554.
- 132 D. P. O'Neal, L. R. Hirsch, N. J. Halas, J. D. Payne and J. L. West, *Cancer Lett.*, 2004, **209**, 171–176.
- 133 C. Loo, A. Lowery, N. J. Halas, J. West and R. Drezeck, *Nano Lett.*, 2005, **5**, 709–711.
- 134 I. H. El-Sayed, X. H. Huang and M. A. El-Sayed, *Cancer Lett.*, 2006, **239**, 129–135.
- 135 X. H. Huang, P. K. Jain, I. H. El-Sayed and M. A. El-Sayed, *Photochem. Photobiol.*, 2006, **82**, 412–417.
- 136 I. Brigger, C. Dubernet and P. Couvreur, *Adv. Drug Delivery Rev.*, 2002, **54**, 631–651.
- 137 V. P. Zharov, E. N. Galitovskaya, C. Johnson and T. Kelly, *Lasers Surg. Med.*, 2005, **37**, 219–226.
- 138 H. Maeda, *Adv. Enzyme Regul.*, 2001, **41**, 187–207.
- 139 P. Jain, I.-H. El-Sayed and M. A. El-Sayed, *Nanotoday*, 2007, **2**, 18–29.
- 140 X. H. Huang, P. K. Jain, I. H. El-Sayed and M. El-Sayed, *Nanomedicine*, 2007, **2**, 681–693.
- 141 X. H. Huang, I. H. El-Sayed, W. Qian and M. A. El-Sayed, *J. Am. Chem. Soc.*, 2006, **128**, 2115–2120.
- 142 H. Takahashi, T. Niidome, A. Nariai, Y. Niidome and S. Yamada, *Chem. Lett.*, 2006, **35**, 500–501.
- 143 T. B. Huff, L. Tong, Y. Zhao, M. N. Hansen, J. X. Cheng and A. Wei, *Nanomedicine*, 2007, **2**, 125–132.
- 144 D. Pissuwan, S. M. Valenzuela and M. B. Cortie, *Biotechnol. Gen. Eng. Rev.*, 2008, **25**, 93–112.
- 145 J. M. Stern and J. A. Cadeddu, *Urol. Oncol.*, 2008, **26**, 93–96.
- 146 Y. T. Lim, M. Y. Cho, B. S. Choi, Y.-W. Noh and B. H. Chung, *Nanotechnology*, 2008, **19**, 375105.
- 147 K. W. Hu, C.-C. Huang, J.-R. Hwu, D.-B. Shieh and C.-S. Yeh, *Chem.-Eur. J.*, 2008, **14**, 2956–2964.
- 148 J. M. Stern, J. Stanfield, W. Kabbani, J.-T. Hsieh and J. A. Cadeddu, *J. Urol.*, 2008, **179**, 748–753.
- 149 Y. Cheng, A. C. Samia, J. D. Meyers, I. Panagopoulos, B. Fei and C. Burda, *J. Am. Chem. Soc.*, 2008, **130**, 10643–10647.
- 150 J. Cardinal, J. R. Klune, E. Chory, G. Jeyabalan, J. S. Kanzius, M. Nalesnik and D. A. Geller, *Surgery*, 2008, **144**, 125–132.
- 151 C. J. Gannon, C. R. Patra, R. Bhattacharya, P. Mukherjee and S. A. Curley, *J. Nanobiotechnol.*, 2008, **6**, 2, DOI: 10.1186/1477-3155-6-2.
- 152 R. Bhattacharya and P. Mukherjee, *Adv. Drug Delivery Rev.*, 2008, **60**, 1289–1306.
- 153 D. L. Chamberland, A. Agarwal, N. Kotov, J. B. Fowlkes, P. L. Carson and X. Wang, *Nanotechnology*, 2008, **19**, 095101.
- 154 V. P. Zharov, K. E. Mercer, E. N. Galitovskaya and M. Smeltzer, *Biophys. J.*, 2006, **90**, 619–627.
- 155 D. Peer, J. M. Karp, S. Hong, O. C. Frarokhzad, R. Margalit and R. Langer, *Nat. Nanotechnol.*, 2007, **2**, 751–760.
- 156 N. L. Rosi, D. A. Giljohann, C. S. Thaxton, A. K. R. Lytton-Jean, M. S. Han and C. A. Mirkin, *Science*, 2006, **312**, 1027–1030.
- 157 P. Ghosh, G. Han, M. De, C. H. Kim and V. M. Rotello, *Adv. Drug Delivery Rev.*, 2008, **60**, 1307–1315.
- 158 G. Han, P. Ghosh and V. M. Rotello, *Nanomedicine*, 2007, **2**(1), 113–123.
- 159 G. Han, P. Ghosh and V. M. Rotello, in *Advanced Experimental Medicine and Biology: Bio-Applications of Nanoparticles*, ed. W. C. W. Chan, Springer, Heidelberg, 2007, vol. 620, ch. 4, pp. 48–56.
- 160 P. H. Yang, X. S. Sun, J. F. Siu, H. Z. Sun and Q. Y. He, *Bioconjugate Chem.*, 2005, **16**, 494–496.
- 161 R. J. Lee and P. S. Law, *Biochim. Biophys. Acta*, 1995, **1233**, 134–144.
- 162 G. F. Paciotti, L. Myer and D. Weinreich, *Drug Delivery*, 2004, **11**, 169–183.
- 163 G. F. Paciotti, D. G. I. Kingston and L. Tamarkin, *Drug Dev. Res.*, 2006, **67**, 47–54.
- 164 P. Nativio, I. A. Prior and M. Brust, *ACS Nano*, 2008, **2**, 1639–1644.
- 165 A. Pal, S. Shah, V. Kulkarni, R. S. R. Murthy and S. Devi, *Mater. Chem. Phys.*, 2009, **113**, 276–282.
- 166 J. L. Li, L. Wang, X.-Y. Liu, Z.-P. Zhang, H.-C. Guo, W.-M. Liu and S.-H. Tang, *Cancer Lett.*, 2009, **274**, 319–326.
- 167 R. K. Visaria, R. J. Griffin, B. W. Williams, E. S. Ebbini, G. F. Paciotti, C. W. Song and J. C. Bischof, *Mol. Cancer Ther.*, 2006, **5**, 1014–1020.
- 168 G. F. Paciotti, D. G. I. Kingston and L. Tamarkin, *Drug Dev. Res.*, 2006, **67**, 47–54.
- 169 G. Han, C. T. Martin and V. M. Rotello, *Chem. Biol. Drug Des.*, 2006, **67**, 78–82.
- 170 K. K. Sanhu, M. M. McIntosh, J. M. Smard, S. W. Smith and V. M. Rotello, *Bioconjugate Chem.*, 2002, **13**, 3–6.
- 171 M. Thomas and A. M. Klibanov, *Proc. Natl. Acad. Sci. U. S. A.*, 2003, **100**, 9138–9143.
- 172 G. Han, N. S. Chari, A. Verma, R. Hong, C. T. Martin and V. M. Rotello, *Bioconjugate Chem.*, 2005, **16**, 1356–1359.
- 173 G. Han, C.-C. You, B.-J. Kim, R. S. Turingan, N. S. Forbes, C. T. Martin and V. M. Rotello, *Angew. Chem., Int. Ed.*, 2006, **45**, 3165–3169.
- 174 Z.-J. Zhu, P. S. Ghosh, O. S. Miranda, R. W. Vachet and V. M. Rotello, *J. Am. Chem. Soc.*, 2008, **130**, 14139–14243.
- 175 Y.-P. Kim, E. Oh, H. K. Shon, D. W. Moon, T. G. Lee and H.-S. Kim, *Appl. Surf. Sci.*, 2008, **255**, 1064–1067.
- 176 P. N. Sisco, C. G. Wilson, E. Mironova, S. C. Baxter, C. J. Murphy and E. C. Goldsmith, *Nano Lett.*, 2008, **8**, 3409–3412.
- 177 X. Li, L. Jiang, Q. Zhan, J. Qian and S. He, *Colloids Surf., A*, 2009, **332**, 172–179.
- 178 S. Dhar, E. M. Reddy, A. Shiras, V. Pokharkar and B. L. V. Prasad, *Chem.-Eur. J.*, 2008, **14**, 10244–10250.
- 179 R. Goel, D. Swanlund, J. Coad, G. F. Paciotti and J. C. Bischof, *Mol. Cancer Ther.*, 2007, **6**, 2039–2047.

- 180 R. Goel, G. F. Paciotti and G. F. Bischof, *Prog. Biomed. Optics Imag. Proceeding of SPIE*, 2008, 68420R.
- 181 E. M. S. Azzam and S. M. I. Morsy, *J. Surf. Deterg.*, 2008, **11**, 195–199.
- 182 P. Diagaradjane, A. Shetty, J. C. Wang, A. M. Elliot, J. Schwartz, S. Shentu, H. C. Park, A. Deorukhar, R. J. Stafford, S. H. Cho, J. W. Tunnell, J. D. Hazle and S. Krishnan, *Nano Lett.*, 2008, **8**, 1492–1500.
- 183 M. Stiti, A. Cecchi, M. Rami, M. Abdaoui, V. Baragan-Montero, A. Scozzafava, Y. Guari, J.-Y. Winum and C. T. Supuran, *J. Am. Chem. Soc.*, 2008, **130**, 16130–16131.
- 184 N. Lewinsky, V. Colvin and R. Drezek, *Small*, 2008, **4**, 26–49.
- 185 C. J. Murphy, A. M. Gole, J. W. Stone, P. N. Sisco, A. M. Alkilany, E. C. Goldsmith and S. C. Baxter, *Acc. Chem. Res.*, 2008, **41**, 1721–1730.
- 186 C. M. Goldman, C. D. McCusker, T. Yilmaz and V. M. Rotello, *Bioconjugate Chem.*, 2004, **15**, 897–900.
- 187 E. Connor, J. Mwamuka, A. Gole, C. J. Murphy and M. Whyatt, *Small*, 2005, **21**, 325–327.
- 188 A. Tkatchenko, H. Xie, Y. Liu, D. Coleman, J. Ryan, W. Glomm, M. Shipton, S. Franzen and D. Feldheim, *Bioconjugate Chem.*, 2004, **15**, 482–490.
- 189 C. H. Hu, H. S. Sheu, C. Y. Pu, J. C. Wang, D. B. Shieh, Y. H. Chen and C. S. Yeh, *J. Am. Chem. Soc.*, 2007, **129**, 2139–2146.
- 190 H. Takahashi, Y. Niidome, T. Niidome, K. Kaneko, H. Kawasaki and S. Yamada, *Langmuir*, 2006, **22**, 2–5.
- 191 T. Niidome, M. Yamagata, Y. Okamoto, Y. Akiyama, H. Takahashi, T. Kawano, Y. Katayama and Y. Niidome, *J. Controlled Release*, 2006, **114**, 343–347.
- 192 M. Hu, J. Chen, Z.-Y. Li, L. Au, G. V. Hartland, X. Li, M. Marquez and Y. Xia, *Chem. Soc. Rev.*, 2006, **35**, 1084–1094.
- 193 N. Pernodet, X. Fang, Y. Sun, A. Bakhtina, A. Ramakrishnan, J. Sokolov, A. Ulman and M. Radfairovitch, *Small*, 2006, **6**, 766–773.
- 194 T. S. Hauck, A. A. Ghazani and W. C. W. Chan, *Small*, 2008, **4**, 153–159.
- 195 R. Gref, P. Couvreur, G. Barratt and E. Mysiakine, *Biomaterials*, 2003, **24**, 4529–4537.
- 196 N. Hillyer and R. Albrecht, *J. Pharm. Sci.*, 2001, **90**, 1927–1937.
- 197 A. E. Hawley, S. Davis and L. Illum, *Adv. Drug Delivery*, 1995, **17**, 129–148.
- 198 P. Maincent, P. Thouvenot, C. Amicabile, M. Hoffman, J. Kreuter, P. Couvreur and J. Devissaguet, *Pharm. Res.*, 1992, **9**, 1534–1539.
- 199 A. Florence, *Pharm. Res.*, 1997, **14**, 259–266.
- 200 G. Zhang, Z. Yang, W. Lu, R. Zhang, Q. Huang, M. Tian, L. Li, D. Liang and C. Li, *Biomaterials*, 2009, **30**, 1928–1936.
- 201 S. Douglas, S. Davies and L. Illum, *CRC Crit. Rev. Ther. Drug Carrier Syst.*, 1986, **3**, 233–261.
- 202 S. Stolnik, L. Illum and S. Davis, *Adv. Drug Delivery Rev.*, 1995, **16**, 195–214.
- 203 G. Sonavane, K. Tomoda, A. Sano, H. Ohshima, H. Terada and K. Makino, *Colloids Surf., B*, 2008, **65**, 1–10.
- 204 G. Sonavane, K. Tomoda and K. Makino, *Colloids Surf., B*, 2008, **66**, 274–280.
- 205 W. H. de Jong, W. I. Hagens, P. Krystek, M. C. Burger, A. J. A. M. Sips and R. E. Geertsma, *Biomaterials*, 2008, **29**, 1912–1919.
- 206 J. M. Farma, M. Puhlmann, P. A. Soriano, D. Cox, G. F. Paciotti, L. Tamarkin and H. R. Alexander, *Int. J. Cancer*, 2007, **120**, 2474–2480.
- 207 E. A. Gratton, P. Polhaus, J. Lee, J. Guo, M. Cho and J. DeSimone, *J. Controlled Release*, 2007, **121**, 10–18.
- 208 M. Semmler-Behnke, W. G. Kreyling, J. Lipka, S. Fertsch, A. Wenk, S. Takenaka, G. Schmid and W. Brandau, *Small*, 2008, **12**, 2108–2111.
- 209 R. Shukla, V. Bansal, M. Chaudhary, A. Basu, R. B. Bhonde and M. Satry, *Langmuir*, 2005, **21**, 10644–10654.
- 210 C. Sönnischen, B. M. Reinhard, J. Liphardt and A. P. Alivisatos, *Nat. Biotechnol.*, 2005, **23**, 741–745.
- 211 J. M. Nam, C. S. Thaxton and C. A. Mirkin, *Science*, 2003, **301**, 1884–1886.